Structure of liquid lithium

2004 J. Phys.: Condens. Matter 16 195

(http://iopscience.iop.org/0953-8984/16/3/002)

INSTITUTE OF PHYSICS PUBLISHING JOURNAL OF PHYSICS: CONDENSED MATTER

J. Phys.: Condens. Matter **16** (2004) 195–222 PII: S0953-8984(04)70750-X

Structure of liquid lithium

Philip S Salmon[1], Ingrid Petri[1], Paul H K de Jong[2], Peter Verkerk[3,6], Henry E Fischer[4] and W Spencer Howells[5]

[1] Department of Physics, University of Bath, Bath BA2 7AY, UK
[2] H H Wills Physics Laboratory, University of Bristol, Royal Fort, Tyndall Avenue, Bristol BS8 1TL, UK
[3] Interfacultair Reactor Instituut, Technische Universiteit Delft, Mekelweg 15, 2629 JB Delft, The Netherlands
[4] LURE, Centre Universitaire Paris-Sud, BP 34, F-91898, Orsay Cédex, France
[5] ISIS, Rutherford Appleton Laboratory, Chilton, Didcot, Oxon OX11 0QX, UK

Received 16 October 2003
Published 9 January 2004
Online at stacks.iop.org/JPhysCM/16/195 (DOI: 10.1088/0953-8984/16/3/002)

Abstract

Neutron diffraction experiments, made at a steady-state reactor source, were used to study the structure of liquid ^{7}Li at temperatures of 197, 452 and 595 °C. A careful data analysis procedure was undertaken in which specific issues taken into account include (i) the influence of Brillouin modes on the measured diffraction pattern at small scattering vectors, (ii) inelasticity corrections that are significant for light atom systems, such as lithium, and (iii) the effects caused by the diffractometer resolution function. Data sets taken for the same liquid temperature using different incident neutron energies yield ion–ion partial structure factors, $S_{\rm II}(k)$, that are in agreement within the statistical errors. The $S_{\rm II}(k)$ are compared with previous experimental results and with the results obtained from liquid state theory and molecular dynamics methods made using several different local pseudopotentials. Finally, the valence electron form factor, $\rho(k)$, is estimated by combining $S_{\rm II}(k)$ with x-ray diffraction data and the ion–valence electron partial structure factor, $S_{\rm Ie}(k)$, is calculated by combining $S_{\rm II}(k)$ with the $\rho(k)$ obtained from both experiment and theory. The results show that the extraction of $\rho(k)$ and $S_{\rm Ie}(k)$ by a combination of neutron and x-ray diffraction methods is feasible in practice, but demonstrates a need for new x-ray diffraction experiments on liquid lithium.

1. Introduction

Liquid lithium has an electronic structure, $1s^2 2s$, which gives it a larger ratio of valence to core electrons than for all other metals, with the exception of beryllium which is, however, an extremely difficult material to study in the liquid phase owing, for example, to its high melting

[6] Deceased.

point of 1278 °C, affinity for oxygen when heated and toxicity [1, 2]. The liquid can be treated as a binary mixture of ions and valence electrons whereby its structure can be described in terms of ion–ion, $S_{\rm II}(k)$, ion–valence electron, $S_{\rm Ie}(k)$, and valence electron–valence electron, $S_{\rm ee}(k)$, partial structure factors, where k denotes the magnitude of the scattering vector [3–5]. The former, $S_{\rm II}(k)$, can be measured directly in a neutron diffraction experiment since the neutrons are scattered by the nuclei and, although they are also scattered by unpaired electrons, this contribution can be neglected: the Pauli paramagnetic susceptibility of the unpaired conduction electrons has a minute size characteristic of diamagnetic materials [6]. By comparison, x-rays are scattered by the electrons and yield a combination of all three partial structure factors. It is then feasible, by following the theory of Chihara [5], to extract $S_{\rm Ie}(k)$ and the valence electron form factor, $\rho(k)$, for a liquid metal by combining the results obtained from neutron and x-ray diffraction experiments.

The structure (ionic and electronic) and dynamics of both liquid and solid lithium have long been the subject of interest and many local [7–11] and non-local [12–18] pseudopotentials have been proposed: the choice of a suitable pseudopotential is an essential first step in the development of most theories for simple liquid metals [19, 20]. In recent years, the static and dynamical properties of liquid lithium have been investigated using a variety of theoretical and computational methods, including the variational modified hypernetted chain (VMHNC) approximation [11, 21, 22] and the quantum hypernetted chain (QHNC) approximation [9, 23] in the integral equation theory of liquid state physics, classical molecular dynamics simulations [17, 18, 24–27] and *ab initio* molecular dynamics simulations made using both the Kohn–Sham [28] and orbital-free [20, 29–31] methods. Reliable experimental results are, therefore, a prerequisite for testing the accuracy of the different potentials together with the different theoretical and computational approaches in which they are employed. Previous diffraction measurements on liquid lithium have shown, however, that the investigation of its structure by experiment involves significant challenges [32].

X-ray diffraction experiments, for example, are not straightforward because the proportion of valence (delocalized) electrons is high and the effect of delocalization on the inelastic Compton scattering is not completely understood [32, 33]. Likewise, neutron diffraction experiments are demanding [34] owing to the relatively large incoherent scattering cross-section of lithium [35], the small mass of the lithium nucleus, which can result in significant and unwanted inelastic scattering effects, and there are potential pitfalls owing to the high sound velocity [36]. This follows since in every neutron diffraction experiment there exists an accessible kinematic range (k, ω) that is dependent on the incident neutron velocity, where $\hbar\omega$ denotes the energy transfer in the neutron–nucleus interaction. The detector in a diffraction experiment performs an integration over the coherent ion–ion dynamical structure factor, $S_{\rm II}(k, \omega)$, along specific pathways which must therefore pass through the main features of $S_{\rm II}(k, \omega)$ if reliable ion–ion static structure factors, $S_{\rm II}(k)$, are to be obtained. Such features include the Brillouin excitations at low-k values which have a position in energy that is determined by the speed of sound [34, 37–40]. Previous reactor-based experiments on liquid lithium were carried out using incident neutrons of wavelength 0.695 Å [33, 41] and, as will be described in section 2, the integration path of the detector does not make a clean cut through the Brillouin modes of $S_{\rm II}(k, \omega)$ at low-k values [34, 42]. Furthermore, in the latter neutron diffraction experiments the incoherent scattering cross-section of lithium was used as an *adjustable* parameter in a method used to ensure that the measured $S_{\rm II}(k)$ has the correct low-k and high-k limits. As will be shown in section 5, the adopted analysis procedure is, however, unsatisfactory and leads to erroneous peak heights.

All of the above provided significant motivation for a new neutron diffraction experiment to study the structure of liquid lithium. A steady-state reactor source was again used but

experiments were carried out using two different incident neutron wavelengths of 0.4962 and 0.7011 Å (corresponding to energies of 332 and 166 meV, respectively) in order to vary, and hence help assess, the effects arising from both the detector integration path and inelastic scattering events. A ^{7}Li sample was selected for the investigation since this isotope is a much weaker absorber of thermal neutrons than ^{6}Li [35]. Furthermore, the experiments were performed at three different temperatures above the melting point of 180.5(1) °C [2, 43][7], namely 197, 452 and 595 °C, with the aim of (i) following the development of the structure with temperature and (ii) checking that the measured low-k limit, $S_{\mathrm{II}}(0)$, obtained from the diffraction experiments at the different temperatures is in agreement with that obtained from isothermal compressibility measurements (see, for example, Squires [44]).

The essential theory required to understand the diffraction results is first given in section 2 and includes an account of, firstly, the relation between the Brillouin excitations and the detector integration path at low k values and, secondly, the inelasticity corrections. The diffraction experiments are then outlined in section 3 along with the data analysis procedure. The results are presented in section 4 where the effect of the diffractometer resolution function is also considered. In section 5, the neutron diffraction results for $S_{\mathrm{II}}(k)$ are compared with those previously obtained from experiment and from the integral equation and molecular dynamics methods made using both the Ashcroft empty core local pseudopotential and a local pseudopotential derived using the neutral pseudoatom (NPA) method. Finally, the results are used in conjunction with the x-ray data of Olbrich *et al* [33] and other data sets to obtain the best estimates of the valence electron form factor, $\rho(k)$, and the $S_{\mathrm{Ie}}(k)$ partial structure factor. A comparison of these functions is made with several of those that have been calculated for liquid lithium and which are available in the literature [9, 18, 22, 23, 30, 45].

2. Theory

The effective differential scattering cross-section per nucleus measured in a neutron diffraction experiment on a single-component system such as lithium is given by [44]

$$\left(\frac{\mathrm{d}\sigma}{\mathrm{d}\Omega}\right)_{\mathrm{eff}} = \left(\frac{\mathrm{d}\sigma}{\mathrm{d}\Omega}\right)_{\mathrm{eff}}^{\mathrm{coh}} + \left(\frac{\mathrm{d}\sigma}{\mathrm{d}\Omega}\right)_{\mathrm{eff}}^{\mathrm{inc}}. \tag{1}$$

For the coherent contribution to the scattering

$$\left(\frac{\mathrm{d}\sigma}{\mathrm{d}\Omega}\right)_{\mathrm{eff}}^{\mathrm{coh}} = \frac{\sigma_{\mathrm{coh}}}{4\pi}\hbar \int_{-\infty}^{\omega_0} \mathrm{d}\omega \, \frac{k_1}{k_0}\eta(k_1) S_{\mathrm{II}}(k,\omega) \tag{2}$$

where $\sigma_{\mathrm{coh}} = 4\pi b_{\mathrm{coh}}^2$ is the bound coherent scattering cross-section of lithium, b_{coh} is the corresponding bound coherent scattering length, $E_0 \equiv \hbar\omega_0$ is the incident energy of the neutrons, k_0 and k_1 are the magnitudes of the incident and scattered wavevectors, respectively (in vector notation $\boldsymbol{k} = \boldsymbol{k}_0 - \boldsymbol{k}_1$), and $\eta(k_1)$ is the detector efficiency. For the incoherent contribution to the scattering:

$$\left(\frac{\mathrm{d}\sigma}{\mathrm{d}\Omega}\right)_{\mathrm{eff}}^{\mathrm{inc}} = \frac{\sigma_{\mathrm{inc}}}{4\pi}\hbar \int_{-\infty}^{\omega_0} \mathrm{d}\omega \, \frac{k_1}{k_0}\eta(k_1) S_{\mathrm{II,inc}}(k,\omega) \tag{3}$$

where $\sigma_{\mathrm{inc}} = 4\pi b_{\mathrm{inc}}^2$ is the bound incoherent scattering cross-section of lithium, b_{inc} is the corresponding bound incoherent scattering length and $S_{\mathrm{II,inc}}(k,\omega)$ is the incoherent ion–ion dynamical structure factor. For a reactor experiment, the measured differential cross-section is, however, determined experimentally by evaluating the integrals of equations (2) and (3) over ω at constant scattering angle 2θ instead of at constant k.

[7] The notation (x) refers to an error of $\pm x$ in the last significant figure(s).

Table 1. Parameters describing liquid lithium at the different temperatures studied in the neutron diffraction experiment. The $S_{\rm II}(k=0)$ limiting values are calculated by using equation (7).

T (°C)	Mass density (g cm^{-3}) [56]	n_0 (Å^{-3})	$c_{\rm s}$ (m s^{-1}) [36]	$\kappa_{\rm T}$ (10^{-10} Pa^{-1}) [63]	$S_{\rm II}(0)$
197	0.5134(1)	0.044 54(1)	4544	1.0247	0.029(2)
452	0.4909(1)	0.042 59(1)	4389	1.1994	0.051(3)
595	0.4771(1)	0.041 39(1)	4301	1.3176	0.065(3)

For molten lithium at sufficiently small k values, $S_{\rm II}(k,\omega)$ comprises a Rayleigh peak centred at $\omega = 0$ and two Brillouin, or sound, peaks centred at $\omega = \pm c_{\rm s}k$, where $c_{\rm s}$ is the speed of sound in the liquid [34, 37–40]. To illustrate the relation between $S_{\rm II}(k,\omega)$ and the integration path of the detector, it is convenient to consider the reduced variables $\omega^* \equiv \omega/\omega_0$ and $k^* \equiv k/k_0$ [46]. Then the position of the sound mode becomes

$$k^* = \frac{v_0}{2c_{\rm s}}\omega^*, \tag{4}$$

where $v_0 = \hbar k_0/m_{\rm n}$ is the incident neutron velocity, $m_{\rm n}$ the neutron mass and the detector integration pathway is given by

$$k^* = [2 - \omega^* - 2\sqrt{1-\omega^*}\cos 2\theta]^{1/2}. \tag{5}$$

These pathways for an incident neutron wavelength, λ, of 0.4962 or 0.7011 Å are compared in figure 1 with the dispersion curves for the Brillouin modes, as calculated from equation (4) by using the $c_{\rm s}$ values from Beyer [36] (see table 1) for the minimum and maximum temperatures investigated experimentally. In addition to the position of the Brillouin mode peaks, the half-width at half-maximum of the peaks is also marked where HWHM $= 6.25k$ meV and k is in units of Å^{-1} [47] such that $k^* = v_0\omega^*/2(c_{\rm s} \pm 950)$. As shown in figure 1, the integration pathway for $\lambda = 0.4962$ Å neutrons cuts cleanly through the Brillouin mode peaks at both temperatures, in contrast to the pathway for $\lambda = 0.7011$ Å neutrons which, having intersected the peak maximum at low k^*, runs approximately parallel to the dispersion curve and does not intersect the lines marking the HWHM. In the case of the latter, the integration of $S_{\rm II}(k,\omega)$ performed by the detector is anticipated to produce a static structure factor, $S_{\rm II}(k)$, which has too high an intensity at low k.

By making the static approximation and taking into account the detector integration pathway [44], the effective differential scattering cross-section given by equation (1) can be rewritten as

$$\frac{1}{\eta(k_0)}\left(\frac{{\rm d}\sigma}{{\rm d}\Omega}\right)_{\rm eff} = b_{\rm coh}^2[S_{\rm II}(k) - 1] + (b_{\rm coh}^2 + b_{\rm inc}^2)[1 + P(k)] \tag{6}$$

where $k = 4\pi \sin\theta/\lambda$ is the magnitude of the scattering vector within the static approximation, $\eta(k_0) = 1 - \exp(-\gamma/k_0)$ is the detector efficiency for incident energy neutrons, γ is the absorption coefficient of the detector; and $P(k)$ is the inelasticity correction, which is significant when energy transfers in the neutron–nucleus interaction, $\hbar\omega$, are non-negligible by comparison with the incident neutron energy E_0. The low-k limit of the static structure factor is given by [44]

$$S_{\rm II}(0) = n_0\chi_{\rm T}k_{\rm B}T, \tag{7}$$

where n_0 and $\chi_{\rm T}$ denote the ionic number density and isothermal compressibility, respectively, the high-k limit of $S_{\rm II}(k)$ is unity and the data should satisfy the sum-rule relation [48]

$$\int_0^\infty {\rm d}k\,[S_{\rm II}(k) - 1]k^2 = -2\pi^2 n_0. \tag{8}$$

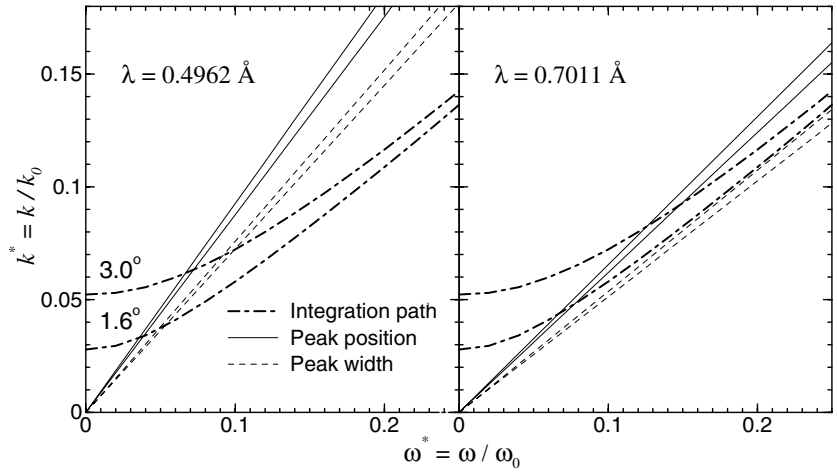

Figure 1. The integration pathway of the detector for $\lambda = 0.4962$ or 0.7011 Å incident neutrons at scattering angles, 2θ, of 1.6° and 3.0° (lower and upper chain curves, respectively) compared with the dispersion curves for Brillouin modes in liquid lithium at temperatures of 197 and 595 °C (lower and upper full straight lines, respectively). The pathways for these 2θ values are nearly symmetrical at small ω^* and are therefore shown only for positive values of this variable. The broken straight lines mark the position of the half-width at half-maximum of the Brillouin mode peaks and for clarity of presentation they are only shown for one side of the peak maxima.

Three different schemes were used to calculate $P(k)$ which, in the case of ^{7}Li, has a large slope owing to the small nuclear mass of 7.016 amu [2]. The resultant correction terms at the lowest temperature of 197 °C used in the neutron diffraction experiments, calculated using $\gamma = 21.54$ Å^{-1}, are compared in figure 2.

In the first scheme of Yarnell *et al* [49], a moments expansion is made of $S_{\rm II}(k,\omega)$ about $\hbar\omega = 0$ and $P(k)$ is given by

$$P(k) = -C_1\frac{E_{\rm rec}}{E_0} + O_2(k) - C_3\frac{E_{\rm rec}}{E_0}\frac{k_{\rm B}T}{E_0} + \frac{m_{\rm n}}{2M}\left(O_2'(k) + \frac{k_{\rm B}T}{E_0}\right) \tag{9}$$

where the functions $O_2(k)$ and $O_2'(k)$ are zero if the correction is made to first order and are given by the expressions $O_2(k) = C_2(E_{\rm rec}/E_0)^2$ and $O_2'(k) = E_{\rm rec}/E_0$ if the correction is made to second order. The recoil energy of the scattering nucleus is $E_{\rm rec} = \hbar^2k^2/2M$, the nuclear mass is M and the constants C_1, C_2 and C_3 are dependent on the detector efficiency: for $\gamma = 21.54$ Å^{-1} they take values of 0.810, 0.152 and 0.256 for the $\lambda = 0.4962$ Å neutrons and 0.881, 0.214 and 0.203 for the $\lambda = 0.7011$ Å neutrons, respectively. Terms proportional to k^2 and k^4 can thereby be identified in the $P(k)$ given by equation (9).

In the second scheme originating from Wick [50], an expansion of $S_{\rm II}(k,\omega)$ is instead made about the recoil energy, $E_{\rm rec}$, and the resultant inelasticity correction to first order is given by the expression [51, 52]

$$\begin{aligned} P(k)+1 = \frac{\eta(k_{\rm rec})}{\eta(k_0)}\Bigg[\frac{M^*}{z}\left(\frac{z+c}{M^*+1}\right)^2 + \frac{k_{\rm B}T}{M^*E_0}\left(\frac{M^*}{z}\right)^3\Bigg\{\frac{1}{2} - \frac{3(M^*-1)s^2}{2z^2} \\ - \frac{(1-A_r)}{(M^*+1)^3}\Bigg[z(M^*-1)(s^2-2cz) + 2zM^*(M^*-c^2) \\ + \frac{1}{2z}(M^*(z+c)^2(M^*-cz+s^2) - c^2s^2(1+2M^*))\Bigg] \end{aligned}$$

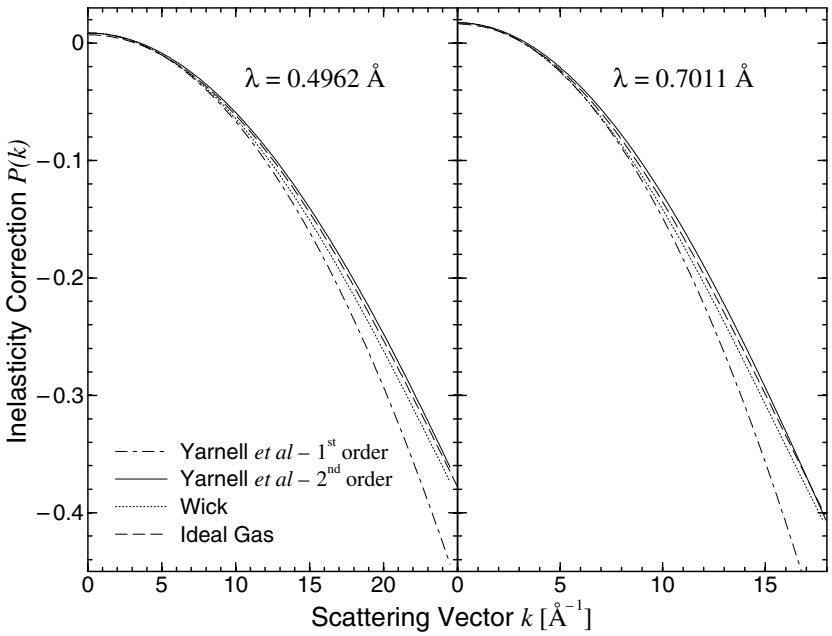

Figure 2. The inelasticity correction $P(k)$ for liquid ^{7}Li at 197 °C obtained by using the three different schemes described in the text for incident neutron wavelengths of 0.4962 and 0.7011 Å: first-order correction after Yarnell *et al* [49] (chain curve); second-order correction after Yarnell *et al* [49] (full curve); correction after Wick [50–52] (dotted curve) and correction after integrating over an ideal gas scattering law [53] (broken curve).

$$-\frac{(B_r - A_r)}{2(M^*+1)^4} M^*(z+c)^2(M^* - cz + s^2)\Bigg\}\Bigg] \tag{10}$$

where $z^2 = (M^*)^2 - s^2$, $s = \sin(2\theta)$, $c = \cos(2\theta)$ and $M^* = M/m_n$ is the reduced mass. A_r and B_r are dependent on the properties of the detector and are given by

$$A_r = 1 - \left(\frac{1}{\eta(k_{rec})} - 1\right)\ln\left(\frac{1}{1-\eta(k_{rec})}\right) \tag{11}$$

$$B_r = A_r + \left(\frac{1}{\eta(k_{rec})} - 1\right)\ln^2\left(\frac{1}{1-\eta(k_{rec})}\right) \tag{12}$$

where $\eta(k_{rec}) = 1 - \exp(-\gamma/k_{rec})$ is the detector efficiency for an energy transfer equal to E_{rec} which corresponds to $k_1 = k_{rec} = k_0(c+z)/(M^*+1)$.

In the third scheme [53], $P(k)$ is evaluated numerically by taking the detector integration pathway through the perfect gas scattering law such that

$$P(k) + 1 = \frac{\hbar}{\eta(k_0)} \int_{-\infty}^{\omega_0} d\omega \, \frac{k_1}{k_0} \eta(k_1) S_{II}(k,\omega) \tag{13}$$

where (see, for example, [44])

$$S_{II}(k,\omega) = \left(\frac{\beta}{4\pi E_{rec}}\right)^{1/2} \exp\left[-\frac{\beta}{4E_{rec}}(\hbar\omega - E_{rec})^2\right], \tag{14}$$

$\beta \equiv (k_B T)^{-1}$ and T is the absolute temperature. Since there are no forces of interaction between the particles in a perfect gas, the coherent and incoherent ion–ion dynamical structure factors, $S_{II}(k,\omega)$ and $S_{II,inc}(k,\omega)$, are identical.

The real-space information corresponding to $S_{\rm II}(k)$ is contained in the partial pair distribution function

$$g_{\rm II}(r) = 1 + \frac{1}{2\pi^2 n_0 r}\int_0^\infty {\rm d}k\,[S_{\rm II}(k) - 1]k\sin(kr) \tag{15}$$

and the mean coordination number of a lithium ion between $r = 0$ and a spherical shell defined by a cut-off radius $r_{\rm c}$ is given by

$$\bar{n}(r_{\rm c}) = 4\pi n_0 \int_0^{r_{\rm c}} {\rm d}r\, r^2 g_{\rm II}(r). \tag{16}$$

3. Experimental method

The diffraction experiments were made using the D4B instrument at the Institut Laue–Langevin (Grenoble, France) on a sample of enriched ^{7}Li (99.99 at.%). The sample was held in a cylindrical vanadium container of 1.31 cm diameter and 0.02 cm wall thickness which was evacuated and sealed by electron beam welding at the Institut für Kerntechnik und Energiewandlung (IKE), Stuttgart. The sample was fully illuminated by a 5 cm high and 1.4 cm wide neutron beam.

At temperatures of 197(3), 452(3) and 595(3) °C, diffraction patterns were measured for (i) the sample in its container in a cylindrical vanadium heater, (ii) a matching empty vanadium container in the vanadium heater and (iii) the empty vanadium heater. The measurements at all three temperatures were made using neutrons of wavelength 0.7011(7) Å, corresponding to the highest attainable neutron flux on D4B and the measurements at the lower and upper temperatures were also made using neutrons of wavelength 0.4962(5) Å, in order to reduce the inelasticity corrections and access a large maximum energy transfer $\hbar\omega_0$. For both incident neutron wavelengths, the mean intensities observed in measurements (i) and (ii) were approximately 5.6 and 2.3 times higher than the mean intensity observed in measurement (iii) for a range of scattering angles where the effect of inelasticity corrections is small. For both wavelengths at room temperature, the diffraction pattern for a cylindrical vanadium rod of diameter 1.0018 cm without the heater was also measured for normalization purposes and the intensity with nothing placed at the beam position was measured to help assess the background count rate. In addition, the intensity for a cadmium neutron absorbing rod in the can and heater at room temperature was measured for both wavelengths to account for the effect of sample self-shielding on the background count rate at small scattering angles [54]. Each complete diffraction pattern was built up from the intensities measured for the different detector groups. These intensities were saved at regular intervals and no deviation between them was observed, apart from the expected statistical variations, which verified the diffractometer stability [55].

For ^{7}Li, $b_{\rm coh} = -2.22(2)$ fm, $b_{\rm inc} = -2.49(5)$ fm and the coherent and incoherent *free* scattering cross-sections used in the data analysis are 0.474(8) and 0.60(2) b, respectively [35]. The absorption cross-section, $\sigma_{\rm abs}$, for ^{7}Li at $\lambda = 1.798$ Å is 0.0454(3) b [35] and its value at other wavelengths was calculated assuming $\sigma_{\rm abs} \propto \lambda$. An adjustment was made to take into account the small but finite contribution (0.01 at.%) from the absorption cross-section of ^{6}Li. The mass density at the different temperatures, taken from Shpil'rain *et al* [56], and the corresponding number density, n_0, are given in table 1.

In the data analysis procedure used to extract $({\rm d}\sigma/{\rm d}\Omega)_{\rm eff}$ from the measured data sets [57], the intensity measured for the empty vanadium heater was treated as a background contribution to the scattering such that

$$\left(\frac{{\rm d}\sigma}{{\rm d}\Omega}\right)_{\rm eff} = \frac{1}{NA_{\rm S,SC}}\left[\left(\frac{I'_{\rm SC}(\theta)}{a(\theta)} - M_{\rm SC}(\theta)\right) - \frac{A_{\rm C,SC}(\theta)}{A_{\rm C,C}(\theta)}\left(\frac{I'_{\rm C}(\theta)}{a(\theta)} - M_{\rm C}(\theta)\right)\right] \tag{17}$$

where $I'_{SC}(\theta)$ and $I'_{C}(\theta)$ represent the measured intensities for the sample (S) in its container (C) and the empty container, respectively, which are normalized to the incident flux and corrected for background scattering. In equation (17), N is the total number of Li nuclei in the neutron beam and the calibration factor $a(\theta)$ was obtained from the vanadium rod intensity $I'_{V}(\theta)$, again normalized to the incident flux and corrected for background scattering, using

$$a(\theta) = I'_{V}(\theta)[A_{V,V}(\theta)N_{V}b^{2}_{inc,V}(1 + P_{V}(k)) + M_{V}(\theta)]^{-1} \tag{18}$$

where N_{V} is the total number of vanadium nuclei in the neutron beam, $b_{inc,V}$ is the bound incoherent scattering length of vanadium [35] and $P_{V}(k)$ is the vanadium inelasticity correction calculated to second order by using equation (9). The $A_{i,j}(\theta)$ are the Paalman and Pings [58] attenuation coefficients and refer to neutrons that are scattered in medium i and attenuated by absorption and scattering in medium(s) j. The $M_{i}(\theta)$ are the multiple scattering cross sections that were calculated in the quasi-static approximation by using the method of Soper and Egelstaff [59]. The $A_{i,j}(\theta)$ and $M_{i}(\theta)$ were calculated using free scattering cross-sections and the correction procedure described by equation (17) ensures that the attenuation corrections are applied to once-scattered neutrons.

It was found that, for the liquid lithium data sets taken using the smallest wavelength neutrons ($\lambda = 0.4962$ Å corresponding to $E_{0} = 332$ meV), the slope on $(d\sigma/d\Omega)_{eff}$ that arises from a departure from the static approximation could best be reproduced, and thereby eliminated, by calculating $P(k)$ to second order using equation (9) (see figure 2). Nevertheless, this equation overestimates the correction at the highest k values, leading to distorted $S_{II}(k)$ for $k > 16$ Å^{-1}. Since the $S_{II}(k)$ show no discernible oscillations arising from ionic ordering in this upper k range, the data sets obtained for the smallest wavelength neutrons were truncated at $k = 16$ Å^{-1}.

By comparison, for the largest wavelength neutrons ($\lambda = 0.7011$ Å corresponding to $E_{0} = 166$ meV) none of the schemes for correcting the inelasticity effects outlined in section 2 proved to be satisfactory, even if an effective nuclear mass was assumed or a variation was allowed for in the detector absorption coefficient γ. An empirical approach had therefore to be adopted and, in the spirit of equation (9), the inelasticity effects were modelled using a polynomial expansion of the form $P(k) = a_{0} + a_{2}k^{2} + a_{4}k^{4}$ [60], where a_{0} was set equal to the $P(0) = k_{B}T/2M^{*}E_{0}$ limit as obtained from equations (9), (10) or (13), while a_{2} and a_{4} were treated as arbitrary coefficients. It was found that the slope on the data arising from inelasticity effects could be satisfactorily modelled up to $k = 14$ Å^{-1}, at which point the data sets for the $\lambda = 0.7011$ Å neutrons were truncated: thereafter the $S_{II}(k)$ show no discernible oscillations arising from ionic ordering. The fitted a_{2} and a_{4} coefficients, in units of 10^{-4} Å^{-2} and 10^{-7} Å^{-4}, are -2.15 and 2.77 for 197 °C, -2.32 and 3.41 for 452 °C and -2.39 and 3.80 for 595 °C, respectively. In the earlier neutron diffraction study of liquid lithium by Olbrich *et al* [33, 41] using $\lambda = 0.695$ Å neutrons, the inelasticity corrections were calculated to *first* order by using equation (9) which also sets a limiting value $P(0) = k_{B}T/2M^{*}E_{0}$.

The static structure factors thus deduced for both neutron wavelengths were found to sit on an incorrect level which necessitated a shift of the data sets by ≈0.11. The source of this problem was investigated by finding the effect on the results of changing the data analysis procedure. For example, the scattering cross-sections were systematically altered, an allowance was made for an error in the sample enrichment and the data were re-analysed from scratch by taking into explicit account the attenuation and multiple scattering caused by the heater whilst treating the intensity with nothing placed at the sample position as the background. It did not prove possible to unambiguously identify the cause of the shifts. However, it is notable that, after the application of a shift, each structure factor has the correct high-k limit, the sum-rule relation of equation (8) is obeyed and the data are consistent with the correct $S_{II}(k \to 0)$

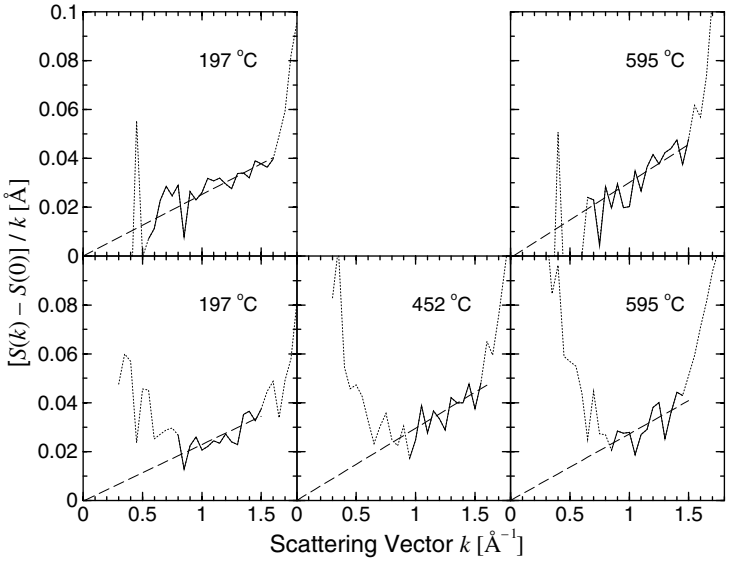

Figure 3. The neutron data for liquid lithium at low-k, plotted as $[S_{II}(k) - S_{II}(0)]/k$ versus k, where the $S_{II}(0)$ values are taken from table 1. The graphs correspond to incident neutron wavelengths of $\lambda = 0.4962$ Å (upper row) and $\lambda = 0.7011$ Å (lower row) and to temperatures of 197, 452 and 595 °C (from left to right). The dotted curves represent the experimental data sets, the full curves show the parts of these data sets chosen to make a straight line fit through the origin and the broken curves show the straight line fits. The rise in intensity at small-k values for the $\lambda = 0.7011$ Å data sets is related to the integration path of the detector over the Brillouin modes, as explained in section 2.

limit as defined by equation (7). Furthermore, after an allowance is made for the effect of the Brillouin modes on the low-k behaviour of the $\lambda = 0.7011$ Å data sets and a correction is applied for the resolution function of the diffractometer (see section 4), the final $S_{II}(k)$ for liquid lithium at a given temperature measured using both neutron wavelengths are found to be in agreement within the statistical errors. Consequently, there was no need to impose any additional scaling of the data, i.e. the calibration factor obtained from the vanadium scattering by using equation (18) was found to be adequate.

4. Results

The low-k region of $S_{II}(k)$ for simple liquid metals is of particular interest since it contains important information on the long-range part of the interionic potential [27, 61, 62]. The structure factor in this low-k region also offers a good guide to the reliability of the applied correction procedures since the measured data should extrapolate to the $S_{II}(k = 0)$ limit given by equation (7), as calculated using the κ_T from Hornung [63] summarized in table 1. In figure 3, the measured data sets in the low-k region are represented in a plot of $[S_{II}(k) - S_{II}(0)]/k$ versus k (see [33, 41, 62]), where the $S_{II}(0)$ values are taken from table 1. The divergence of the $\lambda = 0.7011$ Å data sets from the limiting zero value can be attributed to the integration path of the detector over the Brillouin modes in $S_{II}(k, \omega)$, as shown in figure 1 and described in section 2. By comparison, the $\lambda = 0.4962$ Å data sets tend to the correct thermodynamic limit within the precision shown in figure 3: the observed agreement is not some artefact of an empirical fitting procedure.

To extrapolate the measured $S_{II}(k)$ to small k values, the data in figure 3 were fitted by using a least squares algorithm to a straight line which was constrained to pass through the

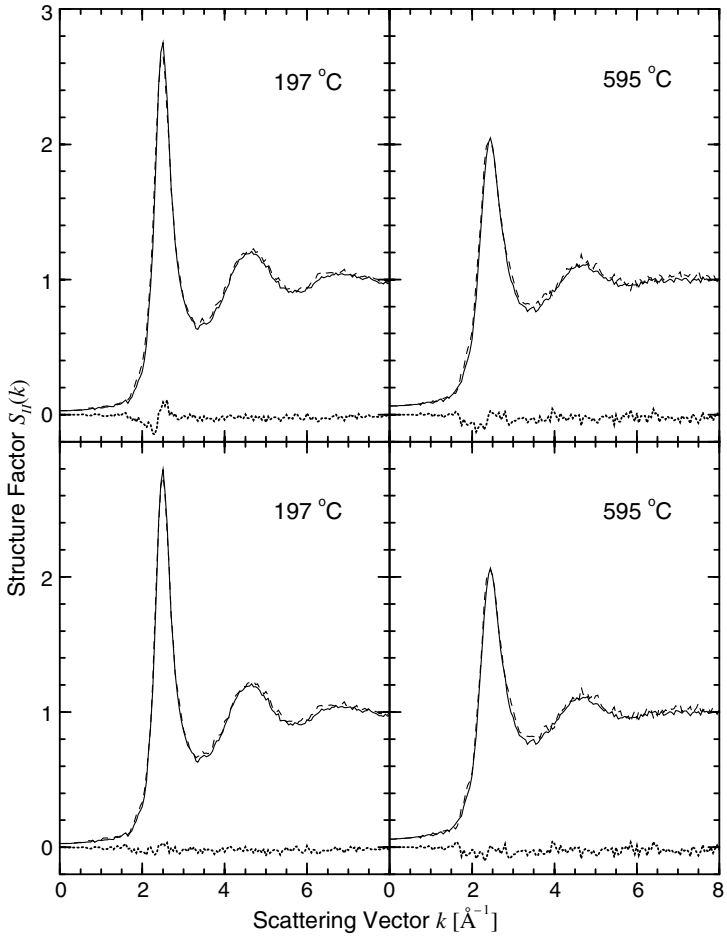

Figure 4. The $S_{\rm II}(k)$ for liquid lithium at 197 and 595 °C measured using incident neutrons of wavelength $\lambda = 0.4962$ Å (broken curves) or $\lambda = 0.7011$ Å (full curves). A comparison is made both before (upper row) and after (lower row) the resolution function correction (see the text). The dotted curves show the differences, $S_{\rm II}(k)$ [$\lambda = 0.7011$ Å] − $S_{\rm II}(k)$ [$\lambda = 0.4962$ Å], between the data sets.

origin, after the erroneous low-k data points for the $\lambda = 0.7011$ Å data sets were omitted along with the noisy data points at the lowest k values for the $\lambda = 0.4962$ Å data sets. As shown in figure 3, the fitted lines are consistent with $S_{\rm II}(k) \propto k^2$ for $k \leqslant 1.5$ Å^{-1} within the experimental error.

A comparison of the $S_{\rm II}(k)$ obtained by using both neutron wavelengths at the lowest temperature of 197 °C is given in figure 4. The functions have the correct low-k and high-k limits and, as shown by the difference between them, they are in agreement within statistical errors over the entire measured k range, except in the region of the first peak at ≈2.48 Å^{-1}. Close inspection of the data sets shows that this discrepancy arises from a small relative shift to lower-k of the first peak for the $\lambda = 0.4962$ Å data set and from a relative lowering of its height. These effects, which are also observed but with reduced magnitude for the $S_{\rm II}(k)$ measured at the highest temperature of 595 °C (see figure 4), can be attributed to the variation with wavelength of the D4B resolution function.

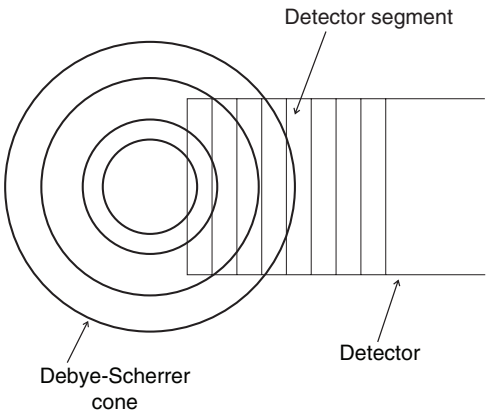

Figure 5. Schematic drawing to illustrate the origin of the 'umbrella effect' at small scattering angles when several diffraction rings of the Debye–Scherrer cone intersect with a single detector segment.

The resolution function of a two-axis diffractometer like D4B is determined by several parameters, including the incident neutron wavelength, the sample dimensions, the detector height and distance from the sample. Depending on the instrument set-up, the resolution function can give rise to a so-called 'umbrella effect' [64, 65] which can be particularly important at small-2θ angles. This effect arises from the intersection of the diffraction rings of the Debye–Scherrer cone with a detector of finite size. When the radius of a ring is small and the detector segments (in this case defined by the cathode wires) are large, each segment can observe intensity from a diffraction ring at 2θ values higher than the scattering angle at which the segment is nominally located (see figure 5). Hence if the diffraction pattern is increasing in intensity with scattering angle, the measured intensity at the nominal angle will be increased while the converse occurs if the scattering intensity is decreasing, i.e. peaks can be asymmetrically broadened and shifted to lower angles. For a liquid, the effect will be significant for sharp peaks in $S_{\mathrm{II}}(k)$ at low-k values, particularly if large samples are used as in the present liquid lithium experiment [65]. The effect also increases with decreasing wavelength since the rings of the Debye–Scherrer cone move closer together.

A correction for the resolution function was made using the 'moments method' of Howells [66] outlined in the appendix. The resolution function of D4B in the set-up corresponding to our experimental conditions was first calculated for a Bragg peak taking into account the sample width and height, the vertical focusing of the incident beam and its horizontal dispersion, the detector height, the sample-to-detector distance and the umbrella effect [65]. Next, the moments of the resolution function were calculated together with the first and second derivatives with respect to the scattering angle 2θ of the static structure factor hitherto obtained and which is now denoted by $I(2\theta)$. The static structure factor, corrected for the resolution function of the diffractometer, is then given by (see equation (A.4))

$$S_{\mathrm{II}}(2\theta) = m_{00}(2\theta)I(2\theta) + \Delta_1(2\theta) + \Delta_2(2\theta) \tag{19}$$

where the remaining symbols are defined in the appendix. As illustrated in figure 6, the main effect of the first and second correction terms, $\Delta_1(2\theta)$ and $\Delta_2(2\theta)$, is to shift and sharpen, respectively, the first peak in the uncorrected structure factor. The comparison in figure 4 shows that the resolution function correction removes most of the initial discrepancy between the data sets measured using the two different wavelengths, especially for the liquid measured

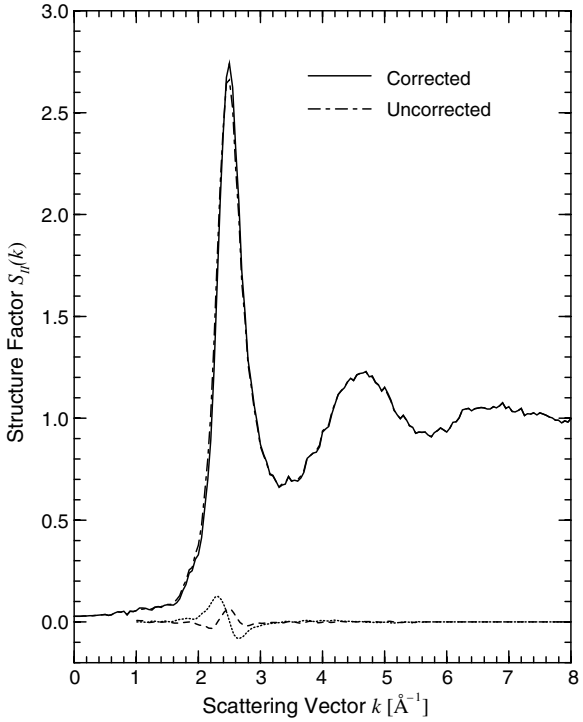

Figure 6. Comparison of the $S_{\rm II}(k)$ for liquid lithium at 197 °C measured using incident neutrons of wavelength $\lambda = 0.4962$ Å both before (chain curve) and after (full curve) the resolution function correction. The first and second resolution function correction terms, Δ_1 and Δ_2, of equation (19) are given by the dotted and broken curves, respectively.

at the lowest temperature of 197 °C for which the correction is largest, owing to the relative sharpness of the first peak in the static structure factor.

The $S_{\rm II}(k)$ for the different wavelengths and temperatures, corrected for the finite resolution function of the D4B diffractometer, are shown in figure 7. The data sets have the correct low-k and high-k limits (the resolution function correction has a significant effect only around the region of the first peak, as shown in figures 4 and 6) and they also obey the sum-rule relation given by equation (8). The corresponding pair distribution functions, given in figure 8, were obtained by truncating the corresponding $S_{\rm II}(k)$ at the *same* maximum value $k_{\rm max} = 14$ Å^{-1} prior to Fourier transformation using equation (15). It was verified that extension of the $\lambda = 0.4962$ Å data set to $k_{\rm max} = 16$ Å^{-1} had no noticeable effect on the $g_{\rm II}(r)$, except in the region of the unphysical low-r oscillations. In this region, the high first positive peak is indicative of a small residual slope on the $S_{\rm II}(k)$ functions, which emphasizes that none of the inelasticity correction schemes defined by equations (9), (10) and (13) are fully adequate for liquid lithium at the neutron wavelengths used in the present work.

5. Discussion

5.1. Temperature dependence of the structure and comparison with previous diffraction studies

As illustrated in figure 9, the peaks in $g_{\rm II}(r)$ for liquid lithium become lower and broader with increasing temperature. The first peak does not, however, shift its position and the

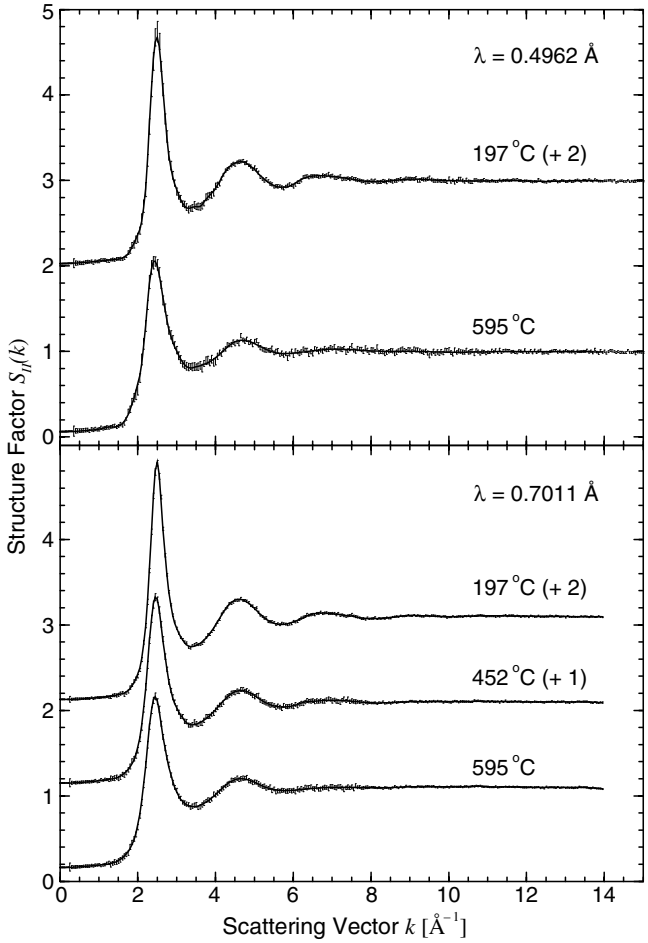

Figure 7. The $S_{\mathrm{II}}(k)$ for liquid lithium obtained by using the full data analysis procedure, including the resolution function correction. The points with error bars give the data points and the full curves give spline fits to the data which were used to obtain the pair distribution functions, $g_{\mathrm{II}}(r)$, represented by the full curves in figure 8.

coordination number obtained from equation (16) by setting the cut-off radius, r_{c}, to the first minimum in $g_{\mathrm{II}}(r)$ remains constant at $\approx$13 (see table 2). At all temperatures, the first peak is also asymmetrical, as shown by reflecting its low-r side about the peak maximum (see the lower inset to figure 9), and the volume change on melting $(V_{\mathrm{l}} - V_{\mathrm{s}})/V_{\mathrm{s}}$, where V_{l} and V_{s} denote the volume of the liquid and solid, respectively, is small at 1.65% [67]. It is therefore tempting to investigate the extent to which the *local* structure of the liquid just above the melting point resembles that of the body-centred cubic (bcc) structure from which the crystal melts, especially as the first symmetrized peak in $g_{\mathrm{II}}(r)$ (represented in the lower inset to figure 9) yields a coordination number of 8.4(4) at 197 °C. However, $g_{\mathrm{II}}(r)$ does not give information on three- or higher-body correlations and the coordination number $\bar{n}(r_{\mathrm{c}})$ is not particularly well defined (see the upper inset to figure 9), e.g. the precise value for the number of nearest neighbours depends on whether r_{c} is chosen to be at the first minimum of $g_{\mathrm{II}}(r)$, $rg_{\mathrm{II}}(r)$ or $r^2 g_{\mathrm{II}}(r)$ (see Pings [68]). Furthermore, the first symmetrized peaks in $rg_{\mathrm{II}}(r)$ and

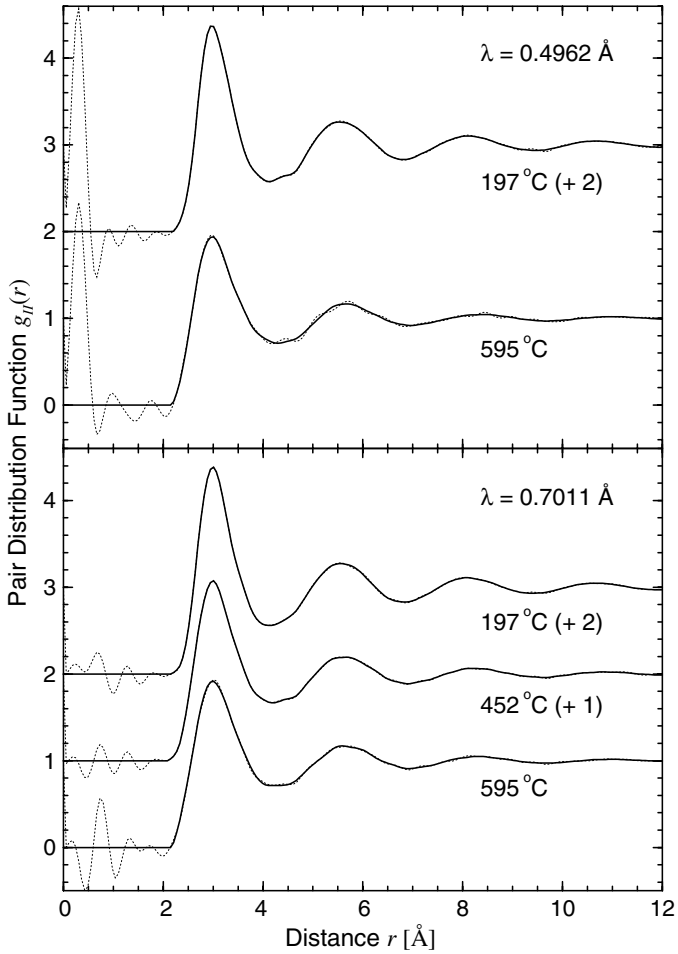

Figure 8. The pair distribution functions, $g_{\rm II}(r)$, for liquid lithium. The broken curves are obtained by direct Fourier transformation of the points with error bars given in figure 7 and the full curves are obtained by Fourier transformation of the spline fits to these data given by the full curves in figure 7. For the latter, the unphysical low-r oscillations are set to zero for r values smaller than the distance of closest approach between the centres of two lithium ions.

$r^2 g_{\rm II}(r)$ yield coordination numbers of 8.8(4) and 9.1(4), respectively, at 197 °C. It is therefore difficult to distinguish between different forms of hard sphere packing [69] in the liquid state from information on $g_{\rm II}(r)$ alone.

In figure 10, the structure factor for liquid lithium at 197 °C measured using $\lambda = 0.7011$ Å incident neutrons is compared with the structure factors measured at a comparable temperature in previous diffraction experiments (these data sets are tabulated by van der Lugt and Alblas [32]). In particular, the new $S_{\rm II}(k)$ differs markedly from that measured in the neutron diffraction experiment of Olbrich *et al* [33] on liquid lithium at 197 °C made using $\lambda = 0.695$ Å incident neutrons. The latter $S_{\rm II}(k)$ is lower in the region 1–2 Å^{-1} and the first peak is much higher, discrepancies which may be attributed in part to use of the lithium incoherent scattering cross-section, $\sigma_{\rm inc}$, as an adjustable parameter in the data analysis procedure [33, 41]. The first peak in $S_{\rm II}(k)$ measured by Olbrich *et al* [33] for

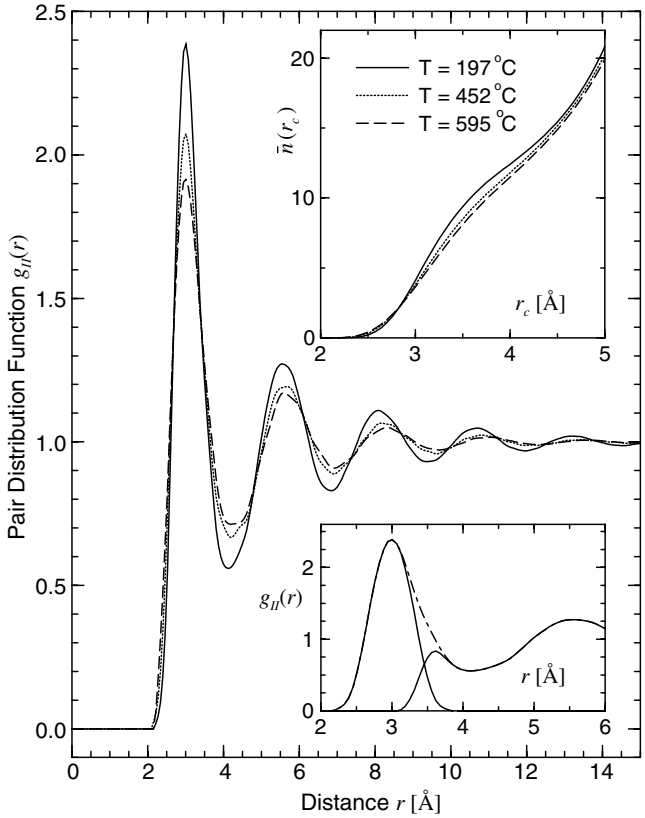

Figure 9. The temperature dependence of the pair distribution function, $g_{\rm II}(r)$, for liquid lithium. The data sets were measured using $\lambda = 0.7011$ Å incident neutrons and the temperatures are 197 °C (full curve), 452 °C (dotted curve) and 595 °C (broken curve). The upper inset shows the corresponding coordination numbers, $\bar{n}(r_{\rm c})$, for different $r_{\rm c}$ values (for a given temperature, the $\bar{n}(r_{\rm c})$ values measured using $\lambda = 0.4962$ Å incident neutrons are nearly indistinguishable on the scale of the plot). The lower inset shows the result of symmetrizing the first peak for the 197 °C data by reflection of its low-r part about the peak maximum.

Table 2. The first, r_1, and second, r_2, peak positions in the $g_{\rm II}(r)$ for liquid lithium at different temperatures together with the coordination number, $\bar{n}(r_{\rm c})$, of the first peak obtained by using equation (16) with $r_{\rm c}$ taken from the first minimum in $g_{\rm II}(r)$. The $g_{\rm II}(r)$ were measured using neutrons with different incident wavelengths λ.

Temperature (°C)	λ (Å)	r_1 (Å)	$\bar{n}(r_{\rm c})$	$r_{\rm c}$ (Å)	r_2 (Å)
197	0.4962	2.97(2)	13.0(5)	4.11	5.52(3)
	0.7011	3.00(2)	13.0(5)	4.11	5.55(3)
452	0.7011	3.00(2)	12.9(5)	4.17	5.68(3)
595	0.4962	2.99(2)	13.1(5)	4.23	5.68(3)
	0.7011	2.99(2)	13.0(5)	4.23	5.59(3)

liquid lithium at 322 °C by using neutron diffraction is also higher than previously measured by Ruppersberg and Egger [70] using the same incident neutron wavelength at the lower temperature of 300 °C. The x-ray structure factor, $S_{\rm X}(k)$, measured by Waseda [71] for liquid lithium at 190 °C exhibits a systematic shift for $k \geqslant 3$ Å^{-1} of the oscillations to higher k values

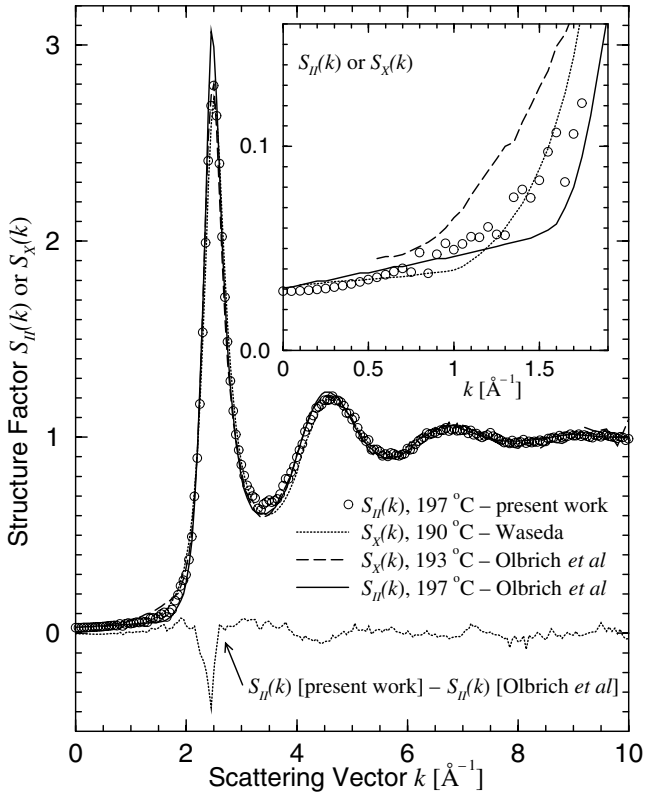

Figure 10. Comparison of the ion–ion structure factor, $S_{\rm II}(k)$, for liquid lithium at 197 °C, measured using incident neutrons of wavelength $\lambda = 0.7011$ Å (open circles), with the structure factors measured in previous diffraction experiments: $S_{\rm II}(k)$ from the neutron diffraction work of Olbrich *et al* [33] at 197 °C (full curve); $S_{\rm X}(k)$ from the x-ray diffraction work of Waseda [71] at 190 °C (dotted curve); $S_{\rm X}(k)$ from the x-ray diffraction work of Olbrich *et al* [33] at 193 °C (broken curve). The dotted curve oscillating about zero gives the difference between $S_{\rm II}(k)$ measured in the present work and $S_{\rm II}(k)$ measured in the work of Olbrich *et al* [33]. The inset shows the low-k region on an expanded scale.

while the $S_{\rm X}(k)$ of Olbrich *et al* [33] at 193(2) °C is higher than for the other structure factors in the range $1.0 \leqslant k$ (Å^{-1}) $\leqslant 1.65$. As will be discussed in section 5.3, differences in the low-k region are nevertheless expected between the fully corrected structure factors measured using neutron and x-ray diffraction.

5.2. The ion–ion structure factor: comparison with molecular dynamics simulations and theoretical calculations

González *et al* [11, 22] studied the structure of liquid lithium, using the variational modified hypernetted chain (VMHNC) approximation in the integral equation theory of liquids, and several of its thermodynamic properties. Many potentials for lithium were used, including the Ashcroft empty core local pseudopotential [7] and a local pseudopotential derived from the neutral pseudoatom (NPA) method [11]. The former contains the core radius as a fitted parameter while the latter has no adjustable parameters. Although the shape of these pseudopotentials is very different, they were found to yield similar overall results for the static

structure factor, $S_{II}(k)$, and the thermodynamics of liquid lithium. Canales *et al* [27] used the Ashcroft empty core and NPA-derived pseudopotentials in classical molecular dynamics simulations of liquid lithium and, by a comparison with experimental results, some features were found that enabled a distinction to be made between them. For example, the NPA-derived pseudopotential led to a better representation of the experimental sound velocity and isothermal compressibility and also gave a structure factor, $S_{II}(k)$, in better agreement with the experimental one at low-k values. Also, the NPA-derived pseudopotential led to a better representation of the dynamical structure factor, $S_{II}(k, \omega)$, measured in the high-resolution inelastic x-ray scattering experiments of Sinn *et al* [38]. It was therefore concluded that the NPA-derived pseudopotential is the more suitable for liquid lithium [38].

The Ashcroft empty core radius of 1.44 au (1 au $\equiv 5.29 \times 10^{-9}$ m) used in the VMHNC calculations, and in the molecular dynamics simulations of Canales *et al* [27], was determined using the *height* of the first peak in $S_{II}(k)$ measured in the neutron diffraction experiment of Olbrich *et al* [33]. As shown in figure 10 there is, however, a clear disagreement between this data set and the $S_{II}(k)$ obtained in the present neutron diffraction work. The new $S_{II}(k)$ for liquid lithium at 197 °C ($\lambda = 0.7011$ Å) was therefore used to derive a new core radius of 1.35 au and the VMHNC calculations and molecular dynamics simulations were repeated [72, 73]. As shown in figure 11, there is a clear improvement in the agreement with the experimental $S_{II}(k)$ at low-k values.

The new $S_{II}(k)$ and $g_{II}(r)$ for liquid lithium at 197 °C ($\lambda = 0.7011$ Å) are shown in figures 12 and 13, respectively, where they are compared, firstly, with the VMHNC and molecular dynamics results obtained using the Ashcroft empty core pseudopotential with the re-parametrized empty core radius [72, 73] and, secondly, with the VMHNC and molecular dynamics results obtained using the NPA-derived pseudopotential [11, 22, 27]. It is found that the molecular dynamics results obtained using the Ashcroft empty core pseudopotential yield the best overall agreement with the experimental $S_{II}(k)$ and $g_{II}(r)$ functions. It would therefore be interesting to simulate the ion–ion *dynamical* structure factor, $S_{II}(k, \omega)$, using the new empty core radius in the Ashcroft potential to investigate the sensitivity of the dynamics to this parameter.

Anta and Madden [30] have also investigated the structure of liquid lithium at 197 and 452 °C by using the orbital-free *ab initio* molecular dynamics simulation method. Their results for $S_{II}(k)$, obtained using two local pseudopotentials labelled 'A' and 'B', which were generated using different approaches of increasing sophistication, are compared with the new neutron diffraction data in figure 14. There is good overall agreement between experiment and simulation for both pseudopotentials, although pseudopotential 'B' is the more successful at the lowest k values, as shown by the comparison for the liquid at 197 °C (see the inset to figure 14). This pseudopotential also leads to a better account of the sound velocity and the measured $S_{II}(k, \omega)$ [38] in the low-k region. Thus, although there are discrepancies with the experimental $S_{II}(k)$ in the region about 2 Å^{-1} (see figure 14), the method used to generate pseudopotential 'B' was preferred by Anta and Madden [30] for constructing local pseudopotentials for orbital-free molecular dynamics simulations.

5.3. The valence electron form factor and the ion–valence electron structure factor

Since Egelstaff *et al* [3] pointed out the possibility of separating the ion–valence electron, valence electron–valence electron and ion–ion correlations in liquid metals by combining the results from three different experimental methods, such as neutron, x-ray and electron diffraction, several attempts have been made to separate these partial correlations [74].

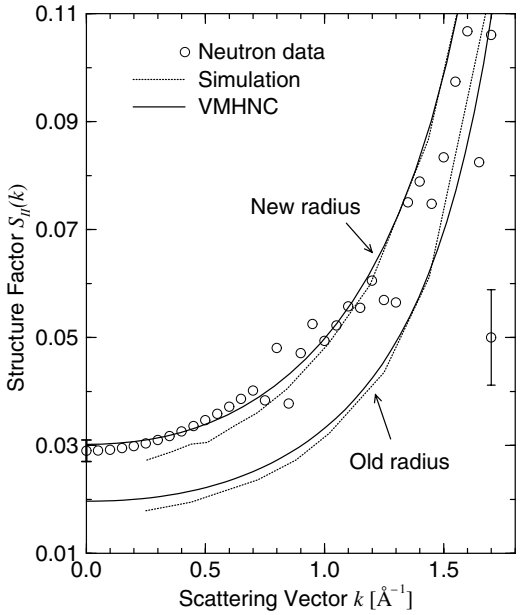

Figure 11. Comparison between the measured and theoretical $S_{\rm II}(k)$ for liquid lithium at 197 °C in the low-k region. The experimental data correspond to the new ($\lambda = 0.7011$ Å) neutron diffraction results (open circles) and the theoretical results were obtained using the Ashcroft empty core pseudopotential with a core radius determined from the height of the first peak in $S_{\rm II}(k)$ taken either from the old neutron diffraction results of Olbrich *et al* [33] (lower set of curves) or from the neutron diffraction results of the present work (upper set of curves). The variational modified hypernetted chain (VMHNC) calculations for the old [11, 22] and new [72] core radii are given by the full curves and the molecular dynamics simulations for the old [27] and new [73] core radii are given by the dotted curves. The $S_{\rm II}(k = 0)$ limit calculated by using equation (7) is given by the point with an error bar at $k = 0$. A representative error bar for the neutron diffraction data is also shown.

Subsequently, Chihara [5] argued that there are both coherent and incoherent contributions to the valence electron–valence electron structure factor, $S_{\rm ee}(k)$, and showed that the ion–valence electron correlations and valence electron form factor should be separable from a combination of only *two* diffraction patterns, namely those measured in neutron diffraction and x-ray diffraction experiments. Some progress along these lines has been made by Takeda and co-workers [75, 76] although the veracity of their results has been called into question [23, 29, 77, 78].

Following Chihara [5], the (Ashcroft–Langreth [79]) ion–valence electron partial structure factor is defined by

$$S_{\rm Ie}(k) = \frac{1}{\sqrt{Z}}\rho(k)S_{\rm II}(k) \tag{20}$$

where Z is the number of valence electrons per ion, $S_{\rm II}(k)$ is the ion–ion structure factor, which is measured directly in a neutron diffraction experiment, and $\rho(k)$ is the valence electron form factor, which is dimensionless. In this formalism the liquid metal is regarded as a system of ions, each having $Z_{\rm I} = Z_{\rm A} - Z$ electrons, where $Z_{\rm A}$ is the atomic number of the corresponding atom, embedded in a uniform background gas of valence electrons, having mean density $n_0^{\rm e} = n_0 Z$ which cancels with the uniform positive background due to the ions so as to satisfy the charge neutrality condition. Each ion attracts its own share of the valence electrons

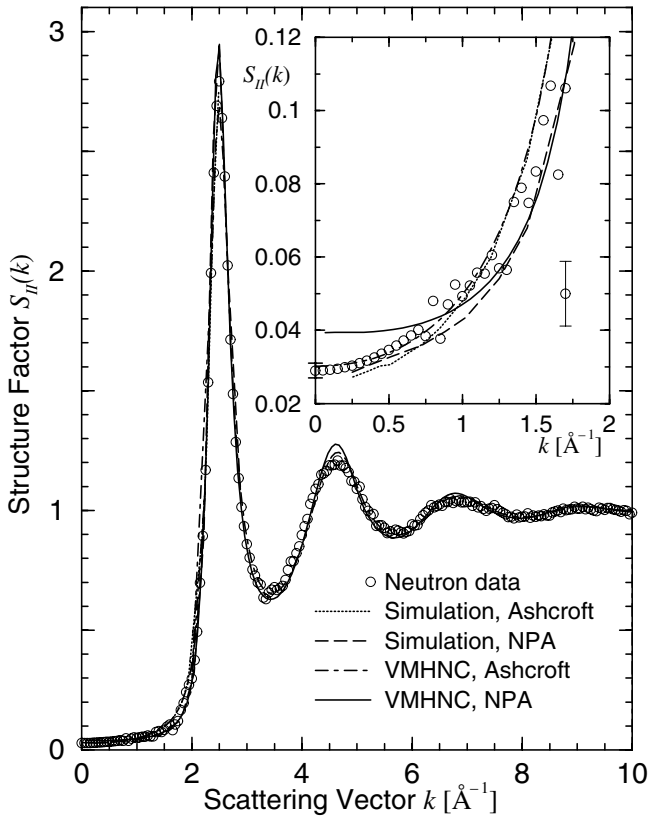

Figure 12. Comparison between the measured and theoretical $S_{\rm II}(k)$ for liquid lithium at 197 °C. The experimental data correspond to the new ($\lambda = 0.7011$ Å) neutron diffraction results (open circles) and the theoretical results were obtained from classical molecular dynamics simulations, made using either the Ashcroft empty core (dotted curve) [73] or neutral pseudoatom (NPA)-derived (broken curve) [27] pseudopotential, and from variational modified hypernetted chain (VMHNC) calculations, made using either the Ashcroft empty core (chain curve) [72] or NPA-derived (full curve) [11, 22] pseudopotential. The Ashcroft empty core radius was derived from the first peak height in the experimental $S_{\rm II}(k)$. The inset shows the low-k region in more detail: the $S_{\rm II}(k=0)$ limit calculated by using equation (7) is given by the point with an error bar at $k = 0$ and a representative error bar for the neutron diffraction data is also shown.

which therefore pile up around the core centre and move with the ion to screen the inter-ionic potentials. Although the screening electrons are not bound to the ion, the system of ion plus screening cloud is sometimes called a pseudoatom and $\rho(k)$ describes the corresponding valence electron distribution in reciprocal space [9, 11, 19, 80]. Within the linear screening approximation [29, 77], the valence electron density at a point, $\rho_{\rm e}(\boldsymbol{r})$, can be written as a sum of the uniform background electron density, $n_0^{\rm e}$, and a superposition of the screening electron density around each ion:

$$\rho_{\rm e}(\boldsymbol{r}) = n_0^{\rm e} + \sum_{\boldsymbol{R}_i} n_{\rm scr}(\boldsymbol{r} - \boldsymbol{R}_i) \tag{21}$$

where $\boldsymbol{R}_i$ denotes the position vector of the ith ion and the screening electron density per ion is defined relative to the uniform background electron density as

$$n_{\rm scr}(\boldsymbol{r}) \equiv \int \frac{{\rm d}\boldsymbol{k}}{(2\pi)^3}\rho(k)\exp({\rm i}\boldsymbol{k}\cdot\boldsymbol{r}) - \frac{n_0^{\rm e}}{N} \tag{22}$$

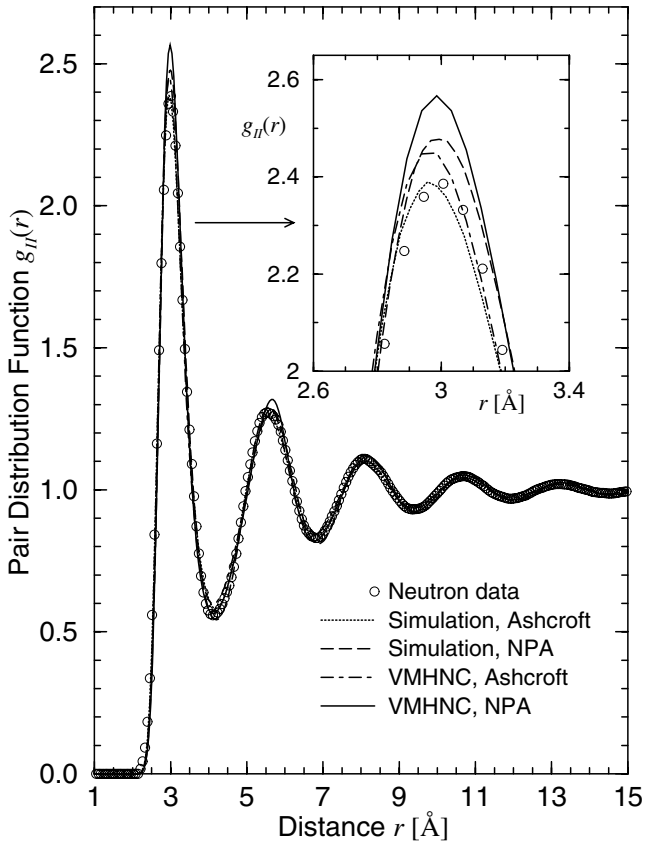

Figure 13. Comparison between the measured and theoretical $g_{\rm II}(r)$ for liquid lithium at 197 °C. The experimental data correspond to the new ($\lambda = 0.7011$ Å) neutron diffraction results (open circles) and the theoretical results were obtained from classical molecular dynamics simulations, made using either the Ashcroft empty core (dotted curve) [73] or neutral pseudoatom (NPA)-derived (broken curve) [27] pseudopotential and from variational modified hypernetted chain (VMHNC) calculations, made using either the Ashcroft empty core (chain curve) [72] or NPA-derived (full curve) [11, 22] pseudopotential. The Ashcroft empty core radius was derived from the first peak height in $S_{\rm II}(k)$ measured in the present work. The inset shows in more detail the region about the first peak maximum.

where $n_0^{\rm e}/N = Z/V$. It then follows that

$$\rho_{\rm e}(\boldsymbol{r}) = \sum_{\boldsymbol{R}_i} \int \frac{{\rm d}\boldsymbol{k}}{(2\pi)^3}\, \rho(k) \exp({\rm i}\boldsymbol{k} \cdot [\boldsymbol{r} - \boldsymbol{R}_i]) \tag{23}$$

where the ρ $(k = 0)$ component corresponds to the uniform electron gas.

The valence electron–valence electron structure factor is given by

$$S_{\rm ee}(k) = \frac{|\rho(k)|^2}{Z} S_{\rm II}(k) + S^0_{\rm ee}(k) \tag{24}$$

where the first term describes the part of the valence electron distribution that is correlated with the ion positions while the second term, $S^0_{\rm ee}(k)$, corresponds to the structure factor of a uniform background gas of valence electrons and gives rise to an incoherent contribution to the scattered intensity that can be measured in an inelastic x-ray (Compton) scattering experiment.

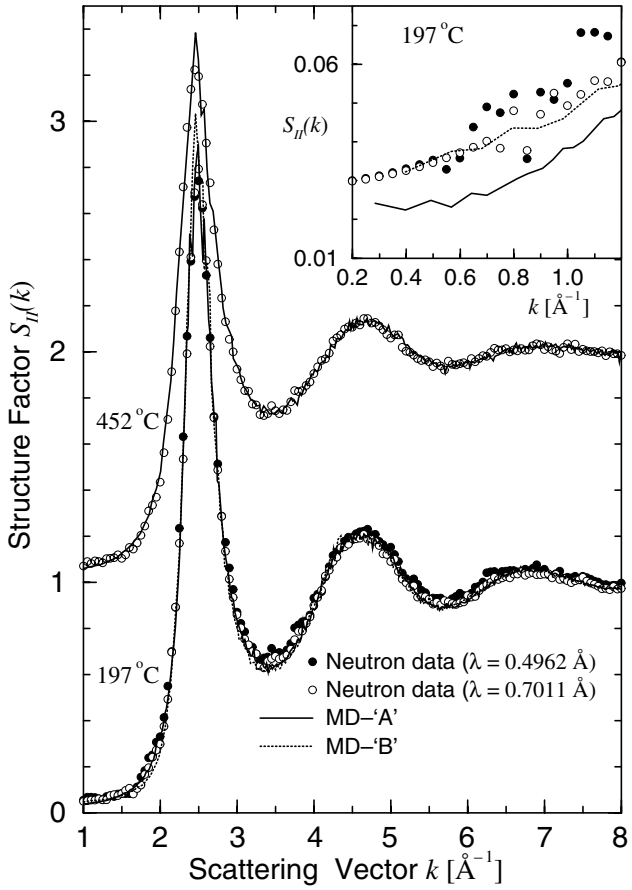

Figure 14. Comparison between the measured and simulated $S_{\mathrm{II}}(k)$ for liquid lithium at temperatures of 197 and 452 °C. The experimental data correspond to the new neutron diffraction results for $\lambda = 0.7011$ Å (open circles) or $\lambda = 0.4962$ Å (full circles). The other results are from the orbital-free *ab initio* molecular dynamics simulations of Anta and Madden [30] for pseudopotential 'A' (full curve) and for pseudopotential 'B' (dotted curve). The data for the 452 °C data set are displaced by unity and the inset displays the low-k region for the 197 °C data set.

Neglecting the forward ($k = 0$) scattering, the intensity per ion measured in an x-ray diffraction experiment on a liquid metal can be written as [5]

$$I_{\mathrm{X}}(k) = |f_{\mathrm{I}}(k)|^2 S_{\mathrm{II}}(k) + 2\sqrt{Z} f_{\mathrm{I}}(k) S_{\mathrm{Ie}}(k) + Z S_{\mathrm{ee}}(k) + Z_{\mathrm{I}} S^{\mathrm{I}}_{\mathrm{inc}}(k) \tag{25}$$

where $f_{\mathrm{I}}(k)$ is the form factor of a metal ion in the liquid. The term $Z_{\mathrm{I}} S^{\mathrm{I}}_{\mathrm{inc}}(k)$ represents the incoherent (Compton) scattering factor of the metal ion and therefore originates from the core electrons. By using equations (20) and (24) it then follows that

$$I_{\mathrm{X}}(k) = |f_{\mathrm{M}}(k)|^2 S_{\mathrm{II}}(k) + Z_{\mathrm{A}} S^{\mathrm{M}}_{\mathrm{inc}}(k) \tag{26}$$

where the form factor of a pseudoatom in the liquid metal is given by

$$f_{\mathrm{M}}(k) = f_{\mathrm{I}}(k) + \rho(k) \tag{27}$$

and its incoherent (Compton) scattering factor is given by

$$Z_{\mathrm{A}} S^{\mathrm{M}}_{\mathrm{inc}}(k) \equiv Z S^{0}_{\mathrm{ee}}(k) + Z_{\mathrm{I}} S^{\mathrm{I}}_{\mathrm{inc}}(k). \tag{28}$$

Often, the x-ray structure factor, $S_X(k)$, of a liquid metal obtained by experiment is published in the form

$$S_X(k) = \frac{I_X(k) - Z_A S^A_{inc}(k)}{|f_A(k)|^2} \tag{29}$$

where $f_A(k)$ and $Z_A S^A_{inc}(k)$ are the form factor and incoherent (Compton) scattering factor, respectively, of a *free* atom. By using equation (26) it hence follows that

$$S_X(k) = \left|\frac{f_M(k)}{f_A(k)}\right|^2 S_{II}(k) + \frac{Z_A(S^M_{inc}(k) - S^A_{inc}(k))}{|f_A(k)|^2}. \tag{30}$$

Provided $S^M_{inc}(k) \approx S^A_{inc}(k)$, the valence electron form factor is then given by

$$\rho(k) \approx \sqrt{\frac{|f_A(k)|^2 S_X(k)}{S_{II}(k)}} - f_I(k) \tag{31}$$

and subtraction of $S_{II}(k)$, as measured in a neutron diffraction experiment, gives

$$S_X(k) - S_{II}(k) \approx \left[\left|\frac{f_I(k)}{f_A(k)}\right|^2 - 1\right] S_{II}(k) + \frac{2 f_I(k)\rho(k) S_{II}(k)}{|f_A(k)|^2} + \frac{|\rho(k)|^2 S_{II}(k)}{|f_A(k)|^2}. \tag{32}$$

The valence electron form factor, $\rho(k)$, was constructed using equation (31) with $S_{II}(k)$ at 197 °C (obtained by averaging the $\lambda = 0.4962$ and 0.7011 Å results in the present work) and $S_X(k)$ at 193(2) °C measured by Olbrich *et al* [33]. In this x-ray diffraction study, the incoherent scattering contribution that originates from inelastic x-ray (Compton) scattering, $S^M_{inc}(k)$, was estimated in a separate experiment during which the energy spectrum of x-rays scattered from solid lithium was measured, i.e. an approximation to $S^M_{inc}(k)$ was used in place of $S^A_{inc}(k)$ in equation (29). The $f_I(k)$ and $f_A(k)$ form factors were taken from tables [81]. As shown in figure 15, $\rho(k)$ tends, within the statistical errors, to the correct low-k limit of unity for lithium. The x-ray data of Waseda [71] for liquid lithium were also used to construct $\rho(k)$ but the resultant function did not have the expected magnitude or shape.

In figure 15, the experimental $\rho(k)$ for liquid lithium is compared with two approximations for this function. The first is constructed by taking the difference between the atom and ion form factors, $[f_A(k) - f_I(k)]$, calculated for *free* lithium [81] and the second is constructed by taking the difference between the pseudoatom and ion form factors for lithium in the *liquid metal*, $[f_M(k) - f'_I(k)]$, as obtained from the calculations of Anta and Louis [23], which were made using the quantum hypernetted chain (QHNC) approximation. At low k there are discrepancies between the two approximations for $\rho(k)$ which cannot be attributed to the ion form factors since $f_I(k) \approx f'_I(k)$. The discrepancies therefore arise from differences between $f_A(k)$ and $f_M(k)$ and show the influence on the free atom form factor of bonding in the liquid state. The experimental $\rho(k)$ is high in the range $\approx$1–1.8 Å^{-1}, which may be traced, by using equation (31), to the x-ray data having a high intensity relative to the neutron data (see figure 10). As pointed out by Olbrich *et al* [33], this may result from an error in the measurement of the inelastic scattering correction $S^M_{inc}(k)$.

Notwithstanding, the experimental data are in better agreement with $\rho(k)$ as calculated for lithium in the liquid metal, i.e. there is a *broader* valence electron density in reciprocal space for a pseudoatom in the metal than for a free atom, which means that in real space the electron distribution at small distances is higher than for the free atom. Theory shows that this enhanced valence electron density at small distances, which is also seen for other simple liquid metals, is accompanied by a reduction of the density at slightly longer distances and by longer-ranged oscillations of the valence electron density about the mean [22, 29, 78].

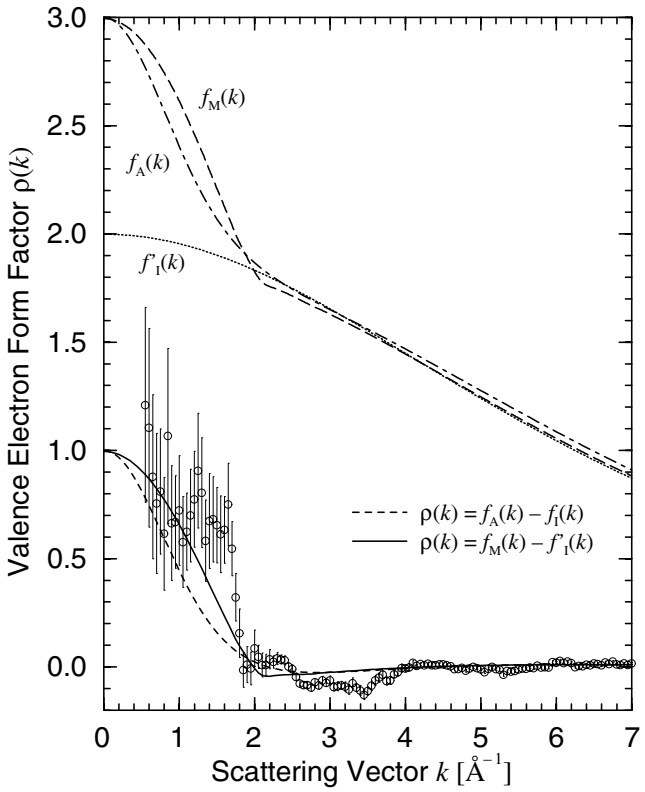

Figure 15. The valence electron form factor, $\rho(k)$, for liquid lithium at 197 °C, shown by the points with error bars, as obtained by combining the new neutron diffraction results with the x-ray diffraction data of Olbrich *et al* [33] according to equation (31). The experimental data are compared with $\rho(k) = [f_A(k) - f_I(k)]$ for *free* lithium (broken curve) and with $\rho(k) = [f_M(k) - f'_I(k)]$ for a pseudoatom in the *liquid metal* (full curve), where $f_A(k)$ (chain curve) and $f_I(k)$ are taken from tables [81] while $f'_I(k)$ (dotted curve) and $f_M(k)$ (long dash curve) are taken from the quantum hypernetted chain (QHNC) results of Anta and Louis [23].

The ion–valence electron partial structure factor, $S_{Ie}(k)$, was constructed using equation (20) with $S_{II}(k)$ at 197 °C (obtained by averaging the $\lambda = 0.4962$ and 0.7011 Å results in the present work) and with $\rho(k)$ taken from the combination of the neutron and x-ray data shown by the points with error bars in figure 15. In view of the uncertainty associated with the experimental $S_X(k)$ used to construct this $\rho(k)$, $S_{Ie}(k)$ was also constructed using two approximations for $\rho(k)$, namely the $[f_A(k) - f_I(k)]$ and $[f_M(k) - f'_I(k)]$ functions given in figure 15. The results are compared in figure 16 with the orbital-free *ab initio* molecular dynamics simulations of Anta and Madden made using pseudopotential 'B' [30] and also with the full QHNC results of Anta and Louis [23].

Firstly, it is notable that the $S_{Ie}(k)$ obtained directly from the experimental data has a magnitude which is considerably smaller than that found in the previous experiments of Takeda *et al* [75, 76] but which is comparable with theoretical expectations. Secondly, whereas the $S_{Ie}(k)$ function that results from using $\rho(k)$ derived from the neutron and x-ray data has notable oscillations, smoother $S_{Ie}(k)$ functions of a diminished magnitude are obtained by using the $\rho(k) = [f_A(k) - f_I(k)]$ and $[f_M(k) - f'_I(k)]$ approximations in equation (20). The oscillations in $S_{Ie}(k)$ that arise from a combination of the neutron and x-ray structure factors

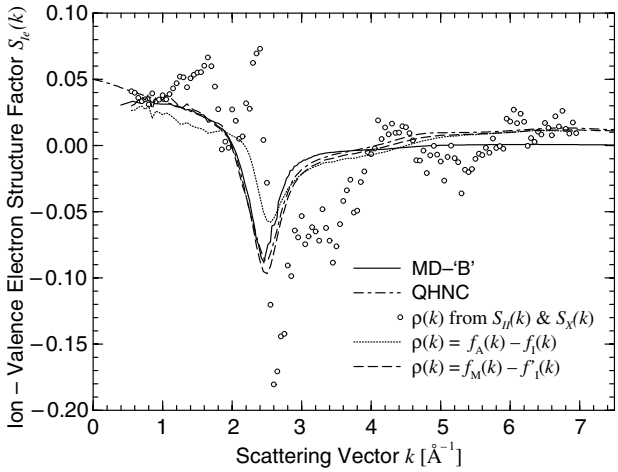

Figure 16. The ion–valence electron partial structure factor, $S_{\mathrm{Ie}}(k)$, for liquid lithium at 197 °C (open circles) obtained by using equation (20) with $S_{\mathrm{II}}(k)$ taken from the present neutron diffraction work and with $\rho(k)$ taken from (a) the combination of $S_{\mathrm{II}}(k)$ with the $S_{\mathrm{X}}(k)$ of Olbrich *et al* [33] shown by the points with error bars in figure 15 (open circles), (b) $\rho(k) = [f_{\mathrm{A}}(k) - f_{\mathrm{I}}(k)]$ taken from tables [81] (dotted curve) or (c) $\rho(k) = [f_{\mathrm{M}}(k) - f'_{\mathrm{I}}(k)]$ for a pseudoatom in the liquid metal taken from Anta and Louis [23] (broken curve). The data are compared with $S_{\mathrm{Ie}}(k)$ obtained from the orbital-free *ab initio* molecular dynamics simulations of Anta and Madden [30] made using pseudopotential 'B' (full curve) and also with the full quantum hypernetted chain (QHNC) results of Anta and Louis [23] (chain curve).

do not, therefore, appear to arise from some inherent problem associated with the neutron diffraction data and ought not to result from the different resolution functions of the neutron and x-ray diffractometers [30]: as shown in section 4, the main effect of the resolution function occurs in the first peak region of the static structure factor. Rather, the oscillations may arise from the approximations used in the analysis of the x-ray diffraction data [5]. Thirdly, there is good overall agreement between the $S_{\mathrm{Ie}}(k)$ obtained by combining the measured $S_{\mathrm{II}}(k)$ with $\rho(k) = [f_{\mathrm{M}}(k) - f'_{\mathrm{I}}(k)]$ (which gives a better representation of the experimental $\rho(k)$—see figure 15) and the $S_{\mathrm{Ie}}(k)$ obtained directly from the full QHNC method. The features of both these $S_{\mathrm{Ie}}(k)$ for $k \leqslant 2.5$ Å^{-1} are also in good agreement with the $S_{\mathrm{Ie}}(k)$ obtained from the orbital-free *ab initio* molecular dynamics simulation although there are notable discrepancies at larger k values. The former results for $S_{\mathrm{Ie}}(k)$, including the appearance of a finite positive value for $S_{\mathrm{Ie}}(k)$ at higher-k values, are supported by the $S_{\mathrm{Ie}}(k)$ calculated by González *et al* [22]. Indeed, according to Louis and Ashcroft [82], the overall shape of these $S_{\mathrm{Ie}}(k)$ is typical of low valence liquid metals ($Z \leqslant 2$) for which $\bar{k}_0 < k_{\mathrm{p}}$, where $\bar{k}_0$ is the first point at which $\rho(k)$ becomes zero with increasing k (≈ 2.0 Å^{-1} in figure 15) and k_{p} is the position of the first peak in $S_{\mathrm{II}}(k)$ (≈ 2.5 Å^{-1} in figure 12).

In summary, the results show that the extraction of $\rho(k)$ and $S_{\mathrm{Ie}}(k)$ by a combination of neutron and x-ray diffraction data following Chihara's approach [5] is feasible in practice but demonstrate a need for new x-ray diffraction experiments on liquid lithium.

6. Conclusions

The ion–ion partial structure factor, $S_{\mathrm{II}}(k)$, for liquid ^{7}Li at temperatures of 197, 452 and 595 °C was measured by using neutron diffraction and the data were carefully analysed to take into account pertinent issues such as (i) the influence of Brillouin modes on the measured diffraction pattern at small scattering vectors, (ii) the accuracy of inelasticity corrections and

(iii) the effect of the diffractometer resolution function. The $S_{II}(k)$ for liquid lithium at a given temperature measured by using different incident neutron energies are in agreement within the statistical errors. The $S_{II}(k)$ are compared with the results obtained from integral equation and molecular dynamics simulations made using the Ashcroft empty core local pseudopotential and also a local pseudopotential derived using the neutral pseudoatom (NPA) method. The newly measured $S_{II}(k)$ pointed to the need for a re-parametrization of the Ashcroft empty core radius and the revised pseudopotential leads to calculated $S_{II}(k)$ that are in good agreement with experiment. It would therefore be interesting to re-calculate the ion–ion *dynamical* structure factor, $S_{II}(k, \omega)$, using this revised pseudopotential to see whether it leads to better agreement with experiment, especially in the low-k region [38]. Finally, the valence electron form factor, $\rho(k)$, was estimated by combining the new experimental $S_{II}(k)$ with the x-ray diffraction data of Olbrich *et al* [33] and the ion–valence electron partial structure factor, $S_{Ie}(k)$, was calculated by combining this $S_{II}(k)$ with the $\rho(k)$ obtained from both experiment and theory. The resultant functions have a magnitude and shape that are comparable with those expected from theory for lithium in the liquid state and hence demonstrate that the experimental extraction of these quantities is feasible in practice. The results do, however, call for new x-ray diffraction experiments on liquid lithium.

Acknowledgments

Special thanks go to many people for making the successful outcome of the present work possible: Pierre Palleau (Grenoble) for assistance with the diffraction experiment, Peter Egelstaff (Guelph) and Alan Soper (ISIS) for help and advice on the inelasticity corrections, Renato Magli (Firenze) for advice on the 'umbrella' effect, Napoleon Anento (Barcelona), Manel Canales (Barcelona) and Luis-Enrique González (Valladolid) for making new and extensive calculations appropriate for the current work and for valuable correspondence, Juan Anta (Oxford) and Ard Louis (Cambridge) for supplying their results and for valuable discussions, and Kozo Hoshino (Hiroshima), Wim van der Lugt (Groningen), Paul Madden (Oxford), Moises Silbert (UEA) and Shin'ichi Takeda (Kyushu) for general help and advice. The provision of a studentship by the University of East Anglia for IP and the support of the EC for the liquid lithium programme are also gratefully acknowledged.

Appendix. Moments method of deconvolution

In a diffraction experiment, the intensity measured by a detector of finite size at scattering angle 2θ will have a contribution from the structure factor at that scattering angle, $S_{II}(2\theta)$, and also from the structure factor at adjacent angles, $S_{II}(2\theta + \rho)$, owing to the finite diffractometer resolution function $R(2\theta, \rho)$. Hence the measured intensity can be written as

$$I(2\theta) = \int R(2\theta, \rho) S_{II}(2\theta + \rho)\, \mathrm{d}\rho \tag{A.1}$$

where ρ is the angular displacement of the detector from the scattering angle 2θ. As shown by Howells [66], the 'moments method' can then be used to deconvolute the structure factor of the liquid from the measured intensity, $I(2\theta)$, when the form of the resolution function is known. By making a Taylor expansion of the structure factor about $S_{II}(2\theta)$ and by taking the first and second derivatives of the measured intensity with respect to the scattering angle,

$I^1 \equiv \mathrm{d}I(2\theta)/\mathrm{d}(2\theta)$ and $I^2 \equiv \mathrm{d}^2 I(2\theta)/\mathrm{d}(2\theta)^2$, it can be shown that

$$\begin{pmatrix} I \\ I^1 \\ I^2 \end{pmatrix} = \begin{pmatrix} M_{00} & M_{01} & M_{02} \\ M_{10} & M_{11} & M_{12} \\ M_{20} & M_{21} & M_{22} \end{pmatrix} \begin{pmatrix} S_{\mathrm{II}} \\ S^1_{\mathrm{II}} \\ S^2_{\mathrm{II}} \end{pmatrix} \tag{A.2}$$

where $S^1_{\mathrm{II}} \equiv \mathrm{d}S_{\mathrm{II}}(2\theta)/\mathrm{d}(2\theta)$ and $S^2_{\mathrm{II}} \equiv \mathrm{d}^2 S_{\mathrm{II}}(2\theta)/\mathrm{d}(2\theta)^2$. The matrix elements $M_{i,j}$ involve the moments of the resolution function, which are defined by

$$M_n \equiv \frac{1}{n!} \int \rho^n R(2\theta, \rho)\, \mathrm{d}\rho \tag{A.3}$$

where n is zero or a positive integer, together with the first and second derivatives of these moments, M^1_n and M^2_n, with respect to the scattering angle 2θ. Specifically $M_{00} = M_0$, $M_{01} = M_1$, $M_{02} = M_2$, $M_{10} = M^1_0$, $M_{11} = (M_0 + M^1_1)$, $M_{12} = (M_1 + M^1_2)$, $M_{20} = M^2_0$, $M_{21} = (2M^1_0 + M^2_1)$ and $M_{22} = (M_0 + 2M^1_1 + M^2_2)$. By inversion of equation (A.2) it then follows that

$$S_{\mathrm{II}}(2\theta) = m_{00} I + m_{01} I^1 + m_{02} I^2 \tag{A.4}$$

where the m_{ij}, which are elements of the inverse matrix M^{-1}, are given by the expressions

$$\begin{aligned} m_{00} &= (M_{11}M_{22} - M_{12}M_{21})/|M| \\ m_{01} &= (M_{02}M_{21} - M_{01}M_{22})/|M| \\ m_{02} &= (M_{01}M_{12} - M_{02}M_{11})/|M| \end{aligned} \tag{A.5}$$

and $|M|$ is the determinant of the matrix. In the case of a sharp peak in the uncorrected intensity, the main effect of the first correction term $\Delta_1 \equiv m_{01} I^1$ will be to shift its position and the main effect of the second correction term $\Delta_2 \equiv m_{02} I^2$ will be to further sharpen its height.

References

[1] Madson W H and Hopkins B S 1939 *Chapters in the Chemistry of the Less Familiar Elements* vol 1, ed B S Hopkins (Champaign, IL: Stipes) chapter 5
[2] Weast R C (ed) 1986 *CRC Handbook of Chemistry and Physics* 67th edn (Boca Raton, FL: CRC Press)
[3] Egelstaff P A, March N H and McGill N C 1974 *Can. J. Phys.* **52** 1651
[4] Dobson P J 1978 *J. Phys. C: Solid State Phys.* **11** L295
[5] Chihara J 1987 *J. Phys. F: Met. Phys.* **17** 295
[6] Ashcroft N W and Mermin N D 1976 *Solid State Physics* (New York: Holt, Rinehart and Winston) p 661
[7] Ashcroft N W 1966 *Phys. Lett.* **23** 48
[8] Hoshino K and Young W H 1986 *J. Phys. F: Met. Phys.* **16** 1659
[9] Chihara J 1989 *Phys. Rev.* A **40** 4507
[10] Das T and Joarder R N 1990 *J. Non-Cryst. Solids* **117/118** 583
[11] González L E, González D J, Silbert M and Alonso J A 1993 *J. Phys.: Condens. Matter* **5** 4283
[12] Dagens L, Rasolt M and Taylor R 1975 *Phys. Rev.* B **11** 2726
[13] Day R S, Sun F and Cutler P H 1979 *Phys. Rev.* A **19** 328
[14] Li D H, Moore R A and Wang S 1987 *J. Phys. F: Met. Phys.* **17** 2007
[15] Walker A B and Taylor R 1990 *J. Phys.: Condens. Matter* **2** 9481
[16] Walker A B and Taylor R 1990 *J. Phys.: Condens. Matter* **2** 9501
[17] Jank W and Hafner J 1990 *J. Phys.: Condens. Matter* **2** 5065
[18] Wax J-F, Jakse N and Bretonnet J-L 1997 *Phys. Rev.* B **55** 12099
[19] Cusack N E 1987 *The Physics of Structurally Disordered Matter* (Bristol: Hilger) p 131
[20] González L E, González D J and López J M 2001 *J. Phys.: Condens. Matter* **13** 7801
[21] González L E, González D J and Silbert M 1991 *Physica* B **168** 39
[22] González D J, González L E and Hoshino K 1994 *J. Phys.: Condens. Matter* **6** 3849
[23] Anta J A and Louis A A 2000 *Phys. Rev.* B **61** 11400
[24] Gonzalez Miranda J M 1985 *Phys. Lett.* A **108** 35

[25] Kambayashi S, Nowotny G, Chihara J and Kahl G 1996 *J. Non-Cryst. Solids* **205–207** 914
[26] Canales M, Padró J A, González L E and Giró A 1993 *J. Phys.: Condens. Matter* **5** 3095
[27] Canales M, González L E and Padró J A 1994 *Phys. Rev.* E **50** 3656
[28] Kresse G 1996 *J. Non-Cryst. Solids* **205–207** 833
[29] Anta J A, Jesson B J and Madden P A 1998 *Phys. Rev.* B **58** 6124
[30] Anta J A and Madden P A 1999 *J. Phys.: Condens. Matter* **11** 6099
[31] González D J, González L E, López J M and Stott M J 2002 *J. Non-Cryst. Solids* **312–314** 110
[32] van der Lugt W and Alblas B P 1985 *Handbook of Thermodynamic and Transport Properties of Alkali Metals* ed R W Ohse (Oxford: Blackwell) p 299
[33] Olbrich H, Ruppersberg H and Steeb S 1983 *Z. Naturf.* a **38** 1328
[34] de Jong P H K, Verkerk P and de Graaf L A 1994 *J. Phys.: Condens. Matter* **6** 8391
[35] Sears V F 1992 *Neutron News* **3** 26
[36] Beyer R T 1985 *Handbook of Thermodynamic and Transport Properties of Alkali Metals* ed R W Ohse (Oxford: Blackwell) p 525
[37] de Jong P H K, Verkerk P and de Graaf L A 1993 *J. Non-Cryst. Solids* **156–158** 48
[38] Sinn H, Sette F, Bergmann U, Halcoussis Ch, Krisch M, Verbeni R and Burkel E 1997 *Phys. Rev. Lett.* **78** 1715
[39] Scopigno T, Balucani U, Cunsolo A, Masciovecchio C, Ruocco G, Sette F and Verbeni R 2000 *Europhys. Lett.* **50** 189
[40] Scopigno T, Balucani U, Ruocco G and Sette F 2000 *J. Phys.: Condens. Matter* **12** 8009
[41] Ruppersberg H and Reiter H 1982 *J. Phys. F: Met. Phys.* **12** 1311
[42] de Jong P H K 1993 *PhD Thesis* Delft University of Technology, The Netherlands
[43] Ohse R W, Babelot J-F, Magill J and Tetenbaum M 1985 *Handbook of Thermodynamic and Transport Properties of Alkali Metals* ed R W Ohse (Oxford: Blackwell) p 329
[44] Squires G L 1978 *Introduction to the Theory of Thermal Neutron Scattering* (Cambridge: Cambridge University Press)
[45] Visser E G, Geertsma W, van der Lugt W and de Hosson J Th M 1980 *Z. Naturf.* a **35** 373
[46] Verkerk P 2001 *J. Phys.: Condens. Matter* **13** 7775
[47] Sinn H and Burkel E 1996 *J. Phys.: Condens. Matter* **8** 9369
[48] Enderby J E, North D M and Egelstaff P A 1966 *Phil. Mag.* **14** 961
[49] Yarnell J L, Katz M J, Wenzel R G and Koenig S H 1973 *Phys. Rev.* A **7** 2130
[50] Wick G C 1954 *Phys. Rev.* **94** 1228
[51] Egelstaff P A and Soper A K 1980 *Mol. Phys.* **40** 569
[52] Egelstaff P A 1987 *Neutron Scattering* (*Methods of Experimental Physics* part B, vol 23) ed D L Price and K Sköld (San Diego, CA: Academic) p 405
[53] Soper A K 1998 private communication
[54] Bertagnolli H, Chieux P and Zeidler M D 1976 *Mol. Phys.* **32** 759
[55] Jal J F, Mathieu C, Chieux P and Dupuy J 1990 *Phil. Mag.* B **62** 351
[56] Shpil'rain E E, Yakimovich K A, Fomin V A, Skovorodjko S N and Mozgovoi A G 1985 *Handbook of Thermodynamic and Transport Properties of Alkali Metals* ed R W Ohse (Oxford: Blackwell) p 435
[57] Salmon P S 1988 *J. Phys. F: Met. Phys.* **18** 2345
[58] Paalman H H and Pings C J 1962 *J. Appl. Phys.* **33** 2635
[59] Soper A K and Egelstaff P A 1980 *Nucl. Instrum. Methods* **178** 415
[60] Bellissent-Funel M-C, Bosio L and Teixeira J 1991 *J. Phys.: Condens. Matter* **3** 4065
[61] March N H and Silbert M 1983 *Phys. Chem. Liq.* **13** 155
[62] Silbert M 1983 *Phys. Chem. Liq.* **13** 75
[63] Hornung K 1985 *Handbook of Thermodynamic and Transport Properties of Alkali Metals* ed R W Ohse (Oxford: Blackwell) p 487
[64] van Laar B and Yelon W B 1984 *J. Appl. Crystallogr.* **17** 47
[65] Finger L W, Cox D E and Jephcoat A P 1994 *J. Appl. Crystallogr.* **27** 892
[66] Howells W S 1984 *Nucl. Instrum. Methods Phys. Res.* **219** 543
[67] Ubbelohde A R 1965 *Melting and Crystal Structure* (Oxford: Clarendon) p 170
[68] Pings C J 1968 *Physics of Simple Liquids* ed H N V Temperley, J S Rowlinson and G S Rushbrooke (Amsterdam: North-Holland) p 386
[69] Wells A F 1984 *Structural Inorganic Chemistry* 5th edn (Oxford: Clarendon) p 141
[70] Ruppersberg H and Egger H 1975 *J. Chem. Phys.* **63** 4095
[71] Waseda Y 1980 *The Structure of Non-Crystalline Materials: Liquids and Amorphous Solids* (New York: McGraw-Hill)
[72] González L E 1999 private communication

[73] Anento N and Canales M 1999 private communication
[74] Tamaki S 1987 *Can. J. Phys.* **65** 286
[75] Takeda S, Inui M, Tamaki S, Maruyama K and Waseda Y 1994 *J. Phys. Soc. Japan* **63** 1794
[76] Takeda S, Kawakita Y, Inui M, Maruyama K, Tamaki S and Waseda Y 1996 *J. Non-Cryst. Solids* **205–207** 365
[77] Hoshino K and Watabe M 1992 *J. Phys. Soc. Japan* **61** 1663
[78] González L E, González D J and Hoshino K 1993 *J. Phys.: Condens. Matter* **5** 9261
[79] Ashcroft N W and Langreth D C 1967 *Phys. Rev.* **156** 685
[80] Ziman J M 1967 *Proc. Phys. Soc.* **91** 701
[81] Maslen E N, Fox A G and O'Keefe M A 1995 *International Tables for Crystallography* vol C, ed A J C Wilson (Dordrecht: Kluwer–Academic) p 476
[82] Louis A A and Ashcroft N W 1998 *Phys. Rev. Lett.* **81** 4456